STRATIFICATION OF CHEMOTHERAPY-TREATED STAGE III COLORECTAL CANCER PATIENTS USING MULTIPLEXED IMAGING AND SINGLE CELL ANALYSIS OF T CELL POPULATIONS

Xanthi Stachtea[1], Maurice B. Loughrey[1,2], Manuela Salvucci[3,4], Andreas U. Lindner[3,4], Sanghee Cho[4], Elizabeth McDonough[4], Anup Sood[4], John Graf[4], Alberto Santamaria-Pang[4], Alex Corwin[4], Pierre Laurent-Puig[5], Sonali Dasgupta[6], Sandra Van Schaeybroeck[1], Mark Lawler[1], Jochen H. M. Prehn[3,4], Fiona Ginty[4] and Daniel B Longley[1#]

Affiliations. [1]Patrick G. Johnston Centre for Cancer Research, School of Medicine, Dentistry and Biomedical Science, Queen's University Belfast, Northern Ireland, UK**.** [2]Department of Cellular Pathology, Royal Victoria Hospital, Belfast Health and Social Care trust, Belfast, UK. [3]Department of Physiology and Medical Physics and Centre for Systems Medicine, Royal College of Surgeons in Ireland (RCSI) University of Medicine and Health Sciences, 123 St. Stephen's Green, Dublin 2, Ireland. [4]GE Research Center, 1 Research Circle, Niskayuna, NY, 12309, USA. [5]UMR-S 1147, Université Paris Descartes, Paris, France. [6]Velindre Cancer Centre, Velindre Rd, Cardiff, UK. [7]Precision Medicine Centre of Excellence, The Patrick G Johnston Centre for Cancer Research, Queen's University, Belfast, Northern Ireland, UK.

[#]***Corresponding author:*** *Daniel B Longley, Patrick G. Johnston Centre for Cancer Research, School of Medicine, Dentistry and Biomedical Science, Queen's University Belfast, Northern Ireland, UK, Phone: +44 (0) 28 9097 2636, Email: d.longley@qub.ac.uk.*

Abstract

Colorectal cancer (CRC) has one of the highest cancer incidences and mortality rates. In stage III, postoperative chemotherapy benefits <20% of patients, while more than 50% will develop distant metastases. Predictive biomarkers for identification of patients with increased risk for disease recurrence are currently lacking, with progress in biomarker discovery hindered by the disease's inherent heterogeneity. The immune profile of colorectal tumors has previously been found to have prognostic value. The aims of this study were to evaluate immune signatures in the tumor microenvironment (TME) using an *in situ* multiplexed immunofluorescence imaging and single cell analysis technology (Cell DIVE^{TM}). Tissue microarrays (TMAs) with up to three 1mm diameter cores per patient were prepared from 117 stage III CRC patients treated with adjuvant fluoropyrimidine/oxaliplatin chemotherapy. Single sections underwent multilplexed immunofluorescence with Cy3- and Cy5-conjugated antibodies for immune cell markers (CD45, CD3, CD4, CD8, FOXP3, PD1) and cell segmentation markers (DAPI, pan-cytokeratin, AE1, NaKATPase and S6). We applied a probabilistic multi-class, multi-label classification algorithm based on multi-parametric models to build statistical models of protein expression to classify immune cells. Expert annotations of immune cell markers were made on a range of images, and Support Vector Machines (SVM) were used to derive a statistical model for cell classification. Images were also manually scored independently by a Pathologist as 'high', 'moderate' or 'low', for stromal and total immune cell content. Excellent agreement was found between manual and total automated scores ($p<0.0001$). Higher levels of multi-marker classified regulatory T cells (CD3+CD4+FOXP3+PD1-) were significantly associated with disease-free survival (DFS) and overall-survival (OS) ($p=0.049$ and 0.032), compared to FOXP3 alone. Our results also showed that PD1- Tregs rather than PD1+ Tregs were associated with improved survival. Overall, compared to single markers, multi-marker classification provided more accurate quantitation of immune cells with greater potential for predicting patient outcomes.

Introduction

For early and locally advanced (stage I and II) colorectal cancer (CRC), the standard treatment of choice for low risk patients is surgical resection. Subsequent oncological treatment decisions for non-metastatic CRC are based largely on the anatomical AJCC/UICC TNM staging classification[1]. After the MOSAIC study in 2004, patients with stage III CRC now commonly receive oxaliplatin/fluoropyrimidine/leucovorin (5-fluorouracil (5FU), FOLFOX; or xeloda/capecitabine, XELOX) as standard adjuvant treatment [2]. Of patients with stage III CRC treated with adjuvant chemotherapy, only ~20% will benefit from adjuvant FOLFOX, and 30% relapse within 2 to 3 years after surgery. Consequently, 80% of patients receive chemotherapy (and endure unnecessary toxicities) that yields no benefit [3]. However, improvements in the understanding of CRC heterogeneity are paving the way for more personalized approaches that combine both histological and molecular data intelligence for patient stratification and therapy selection, including selecting which patients will benefit from adjuvant chemotherapy[4,5].

In the past decade, there has been an increasing interest in the impact of the tumor microenvironment (TME) on patient prognosis. Decreased risk of tumor progression and improved survival have been observed in solid tumors with high T cell infiltration[6]. For CRC, the concept of an “Immunoscore” was introduced by Galon *et al*; this evaluates CD3- and CD8-positive immune infiltrates in the tumor core (TC) and tumor margin (TM) to classify “TNM-immune scores” for tumors[7]. In addition to Immunoscore, there have been numerous studies that reinforce the importance of tumor-infiltrating lymphocytes (TILs) as indicators of prognosis in CRC[8,9]. The importance of the immune contexture in CRC for patient prognosis logically suggests that immunotherapy could be a promising therapeutic approach[10]. Responsiveness to immunotherapy depends on several key factors, including high mutational loads (leading to high levels of tumor neoantigens), which are found in MMR-deficient (dMMR) microsatellite instability-high (MSI-high) CRC[11,12]. The immune checkpoint inhibitor (ICI) pembrolizumab has been approved by the US Food Drug Administration (FDA) for patients

with metastatic dMMR/MSI-high CRC. However, the majority of colorectal tumors are microsatellite stable (MSS), with low mutational burdens and exhibit no response to ICI therapy. Thus, chemotherapy remains the backbone therapy for MSS CRC.

With the unmet clinical need to better stratify stage III patients for possible adjuvant (or neo-adjuvant) chemotherapy and the opportunity to better quantify immune response using newer cell quantification method, our goal was: 1) to compare multi-marker immune cell classification (using Cell DIVE) with immune cell scores determined by a pathologist and 2) investigate the association between single-marker and multi-marker immune cell classification and patient outcomes.

Materials and Methods:

Patient Cohort: Tissue microarrays (TMAs) from formalin-fixed paraffin-embedded (FFPE) tissue blocks with up to three 1mm diameter cores per patient were prepared from 170 patients with stage III CRC. The punches were taken from the center of the tumor based on identification by a pathologist (Prof Manuel Salto-Tellez, Queen's University Belfast). The patient samples were collected from three Research Centres: Beaumont Hospital (RCSI Hospital Group, Ireland), Queen's University Belfast (UK) and Paris Descartes University (France) and the TMAs were constructed at Queen's University Belfast. By design, the TMAs from 91 patients had 2 or 3 cores from each tumor. Pathological stage was determined by the AJCC TNM staging version applicable at the time of the reporting. All Centres provided ethical approval for this study and informed consent was obtained from all participants (NIB12-0034). Patients were recruited during 2005-2012.

At the patient level, the exclusion criteria based on tissue block or clinical data were: i) poor tissue quality or no tumor cells in tissue, ii) loss of follow-up or recurrence and/or death within

less than two months from surgical resection, iii) absence of chemotherapy treatment, iv) positive resection margins, v) tumor site was appendix, vi) stage II or IV disease, vii) only one assessable core remaining after applying all exclusion criteria. At the tissue core level, individual cores on the TMA were excluded for assessment after pathology TMA slide review if no or minimal viable tumor was present for evaluation (i.e. minimal or no tumor tissue, heavily artefacted tissue, extensive tumor necrosis, extensive presence of normal adjacent tissue). After applying exclusion criteria from the original patient cohort, the remaining data comprised 117 stage III patients, who were all treated with 5FU-based adjuvant chemotherapy (predominantly FOLFOX or XELOX).

***KRAS* status:** A MassARRAY system (Sequenom) was used to detect somatic point mutations of *KRAS*.

Multiplexed immunofluorescence analysis of TMAs: Multiplexed immunofluorescence staining of the CRC TMAs was performed as previously described[13] using Cell DIVE™ Cytiva, Issaquah, WA), a multiplexed immunofluorescence microscopy method allowing for multiple protein markers to be imaged and quantified at cell level in a single tissue section. Briefly, formalin-fixed, paraffin-embedded (FFPE) tissue slides were de-paraffinized and rehydrated, underwent a two-step antigen retrieval and were then stained for 1 hour at room temperature using a Leica Bond autostainer. All antibodies were characterized per the previously described protocol[13] and when possible, antibodies in routine clinical use were employed. After down-selection, each antibody was conjugated with either Cy3 or Cy5 bis-NHS-ester dyes using standard protocols as previously described[13]. All sections underwent multiplexed immunofluorescence for a total of 24 markers listed on **Supplementary Table 1**. The markers of interest for this study included CD3, CD4, CD8, FOXP3, CD45, NaKATPase, S6, pan-cytokeratin and AE1 and DAPI nuclear stain. All samples underwent DAPI imaging in every round, and background imaging for the first five rounds and every three rounds thereafter.

Image processing, single cell segmentation: Using Cell DIVE automated image pre-processing software, all images were registered to baseline using DAPI and underwent autofluorescence subtraction, illumination and distortion correction. DAPI and Cy3 autofluorescence images were used to generate a pseudo-colored image, which visually resembles a Hematoxylin and Eosin (H&E) stained image, which we refer to as a virtual H&E (vH&E). This visualization format helps tissue QC review and facilitated review of tumor morphology and lymphocytes. All cells in the epithelial and stromal compartments were segmented using DAPI and pan-cytokeratin, while S6, and NaKATPase were used for subcellular analysis of epithelial cells. Each segmented cell was assigned an individual ID and spatial coordinate, as previously described[13]. Post segmentation, several quality control (QC) steps were conducted, including visual review and manual scoring of tissue quality and segmentation for every image, also described elsewhere[14]. Briefly, each image was reviewed for completeness and accuracy of segmentation masks in each subcellular compartment and tumor and stroma separation. Average biomarker intensity was calculated for each cell and the following additional cell filtering criteria were applied: 1) epithelial cells were required to have either 1-2 nuclei; 2) each sub-cellular compartment (nucleus, membrane, cytoplasm) area had to have > 10 pixels and < 1500 pixels; 3) cells had to have excellent alignment with the first round of staining (round 0) ; 4) cells were at >25 pixels distance from the image margins; 5) cell area for nuclear segmentation mask was >100 or <3000 pixels.

Immune cell classification: A customized machine learning based algorithm[15] developed as a Fiji (ImageJ) plug-in was used for immune cell classification. This is a probabilistic multi-class, multi-label classification algorithms based on multi-parametric models to build statistical models of protein expression and classify immune cells. The images were first segmented into epithelial and stromal regions or masks using a combination of PCK26 and AE1 (expressed in epithelial cells). Nuclei were segmented using DAPI signal and a wavelet-based algorithm[16] and assigned to the epithelium or stromal regions based on co-localization of the nuclei with the epithelial or stromal masks. Manual expert annotations of the following markers associated

with each segmented cell were made: AE1+, CD45+ CD3+, CD4+, CD8+, FOXP3+ and PD1+ and negative cells. Support Vector Machines (SVM) were used to derive a statistical model for cell classification. This multi-marker, annotation driven workflow was custom designed as an FIJI plug-in and allows analysis of complex multi-class models (up to 27 markers)[17,15]. Following classification, counts for both single-marker and multi-marker immune cell types were determined.

Pathologist Scoring: A gastrointestinal pathologist (Maurice B. Loughrey, MBL) performed visual inspection of the virtual H&E slides generated from the DAPI and autofluorescence images[13,18], for the 419 TMA cores. After applying exclusion criteria described earlier, 28 cores were excluded and 391 cores were assessed. MBL assigned two qualitative scores to each core comprising either 'high', 'moderate' or 'low' score, one for stromal cell content and one for immune cell content. For stroma, a high score was assigned when the stromal area was higher than the epithelial area; a moderate score was assigned when the stromal and the epithelial areas were equivalent; and a low score was assigned when the stromal area was lower than the epithelial area. The immune score was based on lymphoid cell abundance in the tissue core.

For equivalent comparison of the pathologist stroma and immune score with Cell DIVE automated scores the following steps were taken: 1) "Stromal cells" were defined as DAPI positive cells that were negative for all markers and outside the epithelial segmentation mask. The stroma score was calculated as the percentage of non-immune stromal cells in all segmented cells in the non-epithelial region; 2) "Immune cells" were defined as segmented cells that were positive for any of the immune markers (CD45, CD3, CD4, CD8) and negative for the AE1 epithelial marker. The immune scores were calculated from the counts of all segmented immune cells. 3) "Epithelial cells" were defined as segmented cells that were positive for AE1 staining and were within the Epithelial Segmentation Mask[19].

Statistical Analysis: For comparison of Cell DIVE quantitative stroma and immune scores with the pathologist scores, the Cell DIVE scores were categorized based on the pathologist's three qualitative groups (high – moderate – low). Statistical analysis for comparison of group means was performed using Welch's ANOVA and pairwise t-test. The association of the single-marker and multi-marker classified immune cells with clinical outcome was evaluated using both univariate and multivariate analyses with adjustment for clinico-pathological confounders (T, N, age, sex, nodal count, positive nodes, lymphovascular invasion, differentiation) in the multivariate Cox proportional hazards models. For the final multivariate models, the variables were subjected to backward elimination and the variables that did not contribute to model fit were removed. The final multivariate model was tested for multi-collinearity and proportional Hazards assumption. Variables with variance inflation factor > 2 were removed, and the remaining variables were re-subjected to backward elimination. The relative quality and goodness-of-fit of models was examined using Harrell's C-index, and the model choice was determined by the Akaike Information Criterion (AIC). The T cell subtypes were counted and analysed as continuous variables after being transformed to 'Percent of total' tissue segmented cells, per patient. When the patients had multiple cores, the average percent of the assessable cores was calculated, unless stated otherwise. For survival analyses, the T cell subtypes calculated as % of total tissue cells were dichotomised at the median, and the Kaplan-Meier method was used to plot survival curves with the log-rank test used for comparisons. No adjustments were made for multiple comparisons. Hypothesis testing was performed at the 5% significance level.

The end-points studied were disease-free survival (DFS) and overall-survival (OS). DFS was the time between the study entry and either the date of the first recurrence, or the date that the last follow-up took place. OS was the time between the date of study entry and either the date of death from any cause, or the date of the last follow-up. All statistical analyses were performed in R Version 3.5.1 (https://cran.r-project.org).

RESULTS

Pathologist scoring versus automated immune cell classification

The TMA cores form the patients were assessed by the pathologist (MBL) and, after exclusion criteria, 62 patients had 3 assessable cores, 99 had 2 assessable cores whereas 7 patients had only 1 assessable core. Intra-tumor heterogeneity was reflected in intra-patient differences between the pathologist's immune and stroma scores. Specifically, from the 62 patients with 3 assessable cores, only 13 (19%) had the same immune score and 18 (29%) the same stroma score for all three cores. For 5 (8%) patients, the immune score was different in each of the three cores, while for 6 (10%) patients, the stroma score was different in each of the three cores. This is to be expected given tumor histology variation in different core punches. From the 99 patients with two cores, 44 (44%) had the same immune score and 42 (42%) had the same stroma score in both tissue cores. In summary, for the 161 patients with more than one core, 104 (65%) showed immune heterogeneity and 101 (63%) showed stroma heterogeneity between their tissue cores. This highlights the inherent high degree of intra-tumor heterogeneity in CRC.

MBL performed visual inspection of the virtual H&E slides and assigned scores to each core of 'high', 'moderate' or 'low', for both stromal and immune cell content. We used the machine learning workflow to create a quantitative cell classification-based immune and stroma score (**Figure 1A**) to compare with the pathologist's scores. The Cell DIVE immune ($p < 0.001$; **Figure 1B**) and stromal ($p < 0.001$; **Figure 1C**) score values were significantly associated with the corresponding pathologist's scores. Therefore, the machine-learning-based Cell DIVE cell classification has potential to be used to evaluate tumor immune and stromal content.

T cell classification for single-marker and multi-marker (multiplexed) classification models. In order to study the impact of different T cell subtypes on patient prognosis in this adjuvant chemotherapy-treated cohort, we used a panel of T cell biomarkers as described

earlier. In addition, to single marker analyses (CD3, CD4, CD8, FOXP3, PD1), multi-marker combinations were used to define subtypes (Tc, TcPD1, Th, ThPD1, Treg, TregPD1, **Figure 2A**). In the single-marker classification workflow, each one of these immune markers was analysed individually, and each segmented cell was classified as either positive or negative for each marker. Since the individual markers are used to generate the multi-marker classification, it is not surprising that they were significantly correlated ($p<0.001$; **Supplementary Figure 3**). The demographic data of the patient cohort are summarized in **Table 1**.

Representative immunofluorescent images of a single tissue core for the individual markers and the corresponding Segmentation Masks are illustrated in **Supplementary Figure 1**. In the multi-marker classification workflow all markers were assessed simultaneously (**Figure 2A(a)**) and, depending on marker co-localization, segmented cells were assigned to the following classes (**Figure 2A(b)**): PD1-negative T-helper (Th), PD1-positive Th (ThPD1), PD1-negative cytotoxic T cells (Tc), PD1-positive Tc (TcPD1), PD1-negative Treg and PD1-positive Treg (TregPD1).

To account for tumor heterogeneity, only patients with more than 1 core were used for the analysis (117 patients). Each T cell subtype was calculated as a percentage of total cells per core and the average percentage per patient was calculated. The distribution of T cell subtypes across the cohort is shown in **Figure 2B**; Tc and TcPD1 cells were the most abundant subtype associated with the epithelial compartment; however, overall and as expected, the majority of each T cell subtype was located in the stroma (**Figure 2C**). All T cell subtypes were generally positively correlated with each other, except TcPD1 had minimal correlation with Th and Treg (**Figure 2D**). Hierarchical clustering was used to assess the immune landscape of the patient cohort (**Figure 2E**). Separation into two clusters, immune "hot" (higher immune cells) and "cold" (lower immune cells), showed that nearly 50% of patients were low in all T cell subtypes; however, Kaplan-Meier analyses showed that their prognosis was similar to patients with higher level of T cells (**Supplementary Figure 2A**).

After separating into three clusters, the "immune-hot" cluster of patients with highest infiltration of T cell subtypes showed improved DFS and OS compared to the other 2 groups that had lower T cell levels; however this did not reach statistical significance (**Supplementary Figure 2B**). Detailed summary statistics for T cells for the multi-marker classifications and single marker classifications are presented in **Table 2**.

In **Supplementary Figure 4** representative images of virtual H&Es, immunofluorescent images and tissue mappings with color-coded cell classifications are illustrated. The selected images are representative of all 9 Stroma-Score/Immune-Score combinations from the pathologist review. This shows that multiplexing can be used to identify multiple subtypes of immune cells simultaneously, allowing for associations and potential cross-talk between distinct cell subtypes in the TME to be assessed.

T cell infiltration and patient prognosis. As proof-of-concept for the applicability of this approach for identification of prognostic immune biomarkers, we next determined the prognostic value of the single and multiplexed markers in this FOLFOX-treated stage III patient cohort. The correlation of each T cell type with clinical endpoints (DFS and OS) was analysed using univariate and multivariate Cox proportional hazards models and Kaplan-Meier analyses.

In the univariate analyses, the forest plots in **Figure 3** demonstrate that none of the single immune markers was significantly associated with DFS (**Figure 3A**) or OS (**Figure 3B**), whereas the level of Treg cells (CD3+/CD4+/FOXP3+/PD1-) from the multi-marker machine-learning classification was significantly associated with longer DFS (*HR = 0.37, 95% CI = 0.14-0.99, p = 0.047*).

For the multivariate analysis, the model initially included the clinical variables: T, N, age, sex, nodal count, positive nodes, differentiation and lymphovascular invasion together with single- and multi-marker immune scores. Backward elimination was used to select variables for the

final model. For DFS in the single-marker model, CD8 remained in the final model and was positively associated with longer DFS (*multivariate adjusted HR = 0.78, 95% CI = 0.6 - 1.0, p = 0.048*; **Figure 3C**) and in the multi-marker model Tregs remained positively associated with longer DFS (*multivariate adjusted HR = 0.34, 95% CI = 0.12 - 1.0, p = 0.049*; **Figure 3C**). For OS in the single-marker model, FOXP3 remained in the final model but did not reach significance (*multivariate adjusted HR = 0.56, 95% CI = 0.297 – 1.06, p = 0.074*; **Figure 3D**) and in the multi-marker model Tregs remained positively associated with longer OS (*multivariate adjusted HR = 0.08, 95% CI = 0.0079 – 0.8, p = 0.032*; **Figure 3D**). The detailed Forest plots for the multivariate models for clinical variables only are shown in **Supplementary Figure 5.**

In order to facilitate comparison with previously published results, Treg levels were divided into high and low groups using the sample median as the cut-off and Kaplan-Meier analyses were performed for curves for DFS and OS (**Figure 3E** and **F**). Similar to the univariate and multivariate analyses above, Treg-*high* patients had improved DFS (*p = 0.019*) and OS (*p = 0.017*) than Treg-*low* patients. Kaplan-Meier curves for all single-marker and multi-marker classes dichotomized on the median are included in **Supplementary Figure 6**. Sub-regional analysis based on the percentage of immune cell subtypes located in the stroma or located within/associated with the epithelial compartment and association with outcome are shown in **Supplementary Table 2**.

T cell infiltration and patient prognosis for immune hot-spot. In order to account for tumor immune heterogeneity, the average percent T cells in multiple cores was used for the above data analyses. However, this could dilute the impact of very high but very localised immune cell infiltrates. We hypothesised that by focusing our analyses on the available cores with *highest* tumor immune regions, we might uncover additional prognostic information; therefore,

we repeated the above analyses for the one core per patient with maximum T cell density for each subtype.

We calculated the total counts of T cells in each core (CD3 counts for single markers and sum of all T cell subtypes for the multiplexed model). From the 117 patients, the cores with the highest number of CD3 or T cells (immune hot-spot core) was selected for further analysis. Cox proportional hazards regression analysis and Kaplan-Meier plots were performed as above. In the univariate analysis none of the single markers was significantly associated with survival. For the multi-marker classification Treg levels were significantly associated with DFS (*HR = 0.51, 95% CI = 0.27-0.97, p = 0.04;* **Figure 4A***)* and were borderline significant for OS (*HR = 0.24, 95% CI = 0.059-1, p = 0.05*; **Figure 4B)**.

In the multivariate analysis, for DFS in the single-marker model, FOXP3 remained in the final model (*multivariate adjusted HR = 0.75, 95% CI = 0.56-1.0, p = 0.05*) and had borderline statistical significance (**Figure 4C**), and in the multi-marker model Treg and TcPD1 remained in the final model and Treg remained statistically significant (for TcPD1: *multivariate adjusted HR = 0.68, 95% CI = 0.38-1.22, p = 0.194;* for Treg: *multivariate adjusted HR = 0.44, 95% CI = 0.20-0.95, p = 0.038).* For OS, none of the single markers remained in the final model. In the multi-marker model, Treg levels remained in the final model and were significantly associated with improved OS (*multivariate adjusted HR = 0.14, 95% CI = 0.026-0.78, p = 0.025*) (**Figure 4D**).

As previously, Kaplan-Meier curves for all single marker and multi-marker classes dichotomized on the median are included in **Supplementary Figure 7.** Sub-regional analysis based on the percentage of immune cell subtypes located in the stroma or located within/associated with the epithelial compartment and association with outcome are shown in **Supplementary Table 3.**

Association of *KRAS* status with survival and distribution of T cell subtypes. In adjuvant FOLFOX/XELOX-treated stage III colorectal cancer patients, *KRAS* mutations have been associated with shorter time to recurrence (TTR) and OS[20]. We performed survival analysis for the patients with known *KRAS* status (108 out of 117 patients tested) to study the effect of this mutation in our cohort and its interaction with T cell subtype levels. Survival curves for colorectal cancer DFS and OS were plotted using the Kaplan-Meier method and compared by the log rank test using the *KRAS* mutation status as the stratification variable. *KRAS* status was not significantly associated with prognosis in our cohort, although, interestingly, there was a non-significant trend (p = 0.07) for *KRAS* mutant tumors to be associated with better DFS in this FOLFOX-treated cohort (**Supplementary Figure 8**). *KRAS* mutation has also been reported to have an immunosuppressive effect in the tumor microenvironment of colorectal cancer[21]. Summary statistics for the clinicopathological data of the patients grouped by *KRAS* status are shown in **Table 3**. No differences of T cell subtypes were observed between *KRAS* WT and mutant patients, for any of the classes tested for multiplexed classification or single marker classification. Collectively, these results indicate that the prognostic impact of T cell subtypes is not associated with *KRAS* mutational status.

DISCUSSION

Currently 5FU-based chemotherapy (usually FOLFOX or XELOX) is used as adjuvant treatment for stage-III CRC patients[2]. However, only 20% of patients benefit, while 30% will experience recurrence[3]. Therefore, reliable biomarkers that can predict which stage III patients would benefit from adjuvant chemotherapy is an urgent unmet clinical need in CRC.

A large number of multigene signatures using tumor gene expression profiles have emerged in the last decade, such as Consensus Molecular Subgroups (CMS) and CRC Intrinsic Subtypes (CRIS), which classify patients into molecular subtypes for risk prediction[22,23,24]. However, this approach is therapeutically valuable only under the assumption that highest risk

patients will also be the most responsive to chemotherapy. This is not the case and, in fact, CMS4 patients who are predicted to have poor prognosis do not benefit from intensive adjuvant chemotherapy[25]. We recently reported that stage-II patients with CMS2/CRIS-C tumors, which demonstrate low levels of CD8-positive tumor-infiltrating lymphocytes benefit from adjuvant chemotherapy. In stage III patients, benefit from chemotherapy was particularly apparent in CMS2/CRIS-C and CMS2/CRIS-D patients[5]. However, transcriptional profiling is not routinely available or applied in clinical practice. Ideally, a clinical test to triage patients for adjuvant chemotherapy that could be performed rapidly on a single FFPE tumor section would be extremely useful.

Herein, we explored the potential of the Cell DIVE platform for enumerating several key immune cell populations previously linked with patient outcome in CRC. Using FFPE tissue samples, Cell DIVE can measure up to 60 markers within a single histological section, whereas standard IHC would require multiple sections to achieve similar result. This requirement would introduce the problem of cellularity changes through the sequential sections, as well as require extensive use of often limited valuable biological material. In addition, with Cell DIVE, multiple markers can be visualized simultaneously, thus increasing specificity for cell classification and providing a molecular signature within a histological content. In concert with user-friendly machine-learning methodologies, Cell DIVE has the potential to become a routine digital pathology platform for clinical laboratory settings. To demonstrate this, we compared immune and stroma scoring from the visual inspection of all tissues by a gastrointestinal pathologist with the corresponding Cell DIVE-derived immune and stroma scoring. Cell DIVE scoring showed significant association with the pathologist's scores, suggesting that the Cell DIVE platform provides robust immune and stroma scoring for tumor tissue sections.

Using the Cell DIVE platform and a segmentation and classification workflow involving 10 markers, we show that we were able to detect 6 classes of T cells and associate them with patient prognosis using a single section from TMAs of FOLFOX/XELOX-treated stage III

patients. Our results showed that high levels of Treg cells (CD3+/CD4+/FOXP3+/PD1-) were associated with improved survival in this cohort and were distinct from their PD1+ counterparts.

Treg cells are key mediators of self-tolerance, regulating multiple immune cells, such as CD4+ and CD8+ effector cells, macrophages and dendritic cells[26]. In the thymus, CD25+/CD4+ thymocytes can become Treg precursors, which, after stimulation with IL-2 and TGF-β, will differentiate into natural thymic FOXP3+ Tregs[27,28]. Natural Tregs can recognize self-antigens and migrate to damaged tissues to supress the activity of other T cells and prevent an uncontrolled inflammatory response[29,30]. Outside the thymus, in secondary lymphoid organs and peripheral tissues, Tregs are derived from differentiation of naïve conventional CD4+ T cells in response to cytokines that induce FOXP3 expression[31,32]. In CRC, there are higher levels of Tregs in the tumor than in healthy tissue. Recently, it has been shown that tumor-associated Tregs have distinct differences from normal peripheral Tregs[33,34]. In cancer, Tregs can suppress anti-tumor immune responses[35] or have protective roles by controlling cancer-associated inflammation[36,37]. Within the intestine, immune cells reside within the mucosa[38] and are tightly associated with the intestinal microbiome, thus intestinal Treg depletion can lead to unresolved inflammation[28,36].

High Treg levels have been associated with poor clinical outcomes in different cancers, including CRC[35,39,40], in contrast to our findings; other studies have associated high Treg levels with better prognosis in CRC patients[41,42,43,44,45]. There are a number of reasons that could be responsible for these apparently contradictory results. For example, differences in the study cohorts, most notably, stage and whether patients were treated with chemotherapy, but also cohort size, variable thresholds for scoring, technical differences in detection and scoring between laboratories and different follow-up times[46] may contribute to these findings. In addition, the conflicting results may be due to lack of robust biomarkers that can reflect the Treg versatility and plasticity, and the best classification method for Treg is still under active debate. FOXP3 is a biomarker with high selectivity for Treg identification that is routinely used

as a Treg biomarker in clinical studies. However, it has limitations since it is not exclusively expressed by Treg cells. FOXP3 can also be expressed in dividing, activated T effector cells[47,48]. Apart from FOXP3, some Treg subtypes can express other molecules that increase their immuno-suppressive capacity, and these highly suppressive Treg cells have been detected in CRC patients[49,50,51]. Therefore, relying solely on FOXP3 as a marker of Tregs may be the cause of some of the inconsistencies in the literature regarding Treg and CRC prognosis.

Recently, it was shown that the majority of intra-tumoral T cells in the TME are CD4+ with co-expression of PD1 molecules[52,53], which is similar to our findings. PD-1 expression on T cells can be sign of early activation or exhaustion and reduced effector functions, due to prolonged exposure to tumor antigens[54]. Our results show that PD1- Tregs rather than PD1+ Tregs are associated with improved survival. Overall, the presence of Treg correlates with the presence of T effector cells in inflamed tissues. Given that CRC is a highly inflammatory type of tumor, PD1-Treg enrichment may not be associated with pro-tumorigenic immunosuppression, but rather are recruited as a result of an active immune response; this would explain the association which we observed with improved prognosis in this chemotherapy-treated stage-III cohort. Lastly, one limitation of our study is the lack of untreated patients for comparison. Therefore, we cannot evaluate the potential of Tregs as a prognostic biomarker. Of note, Tregs have been associated with better prognosis both for treated[41] and untreated patients[55].

The association of T cell infiltration with patient prognosis was assessed using: i) the average of two or three available TMA cores, and ii) the core with the highest T cell infiltration (or the "immune hot-spot" core). While using the core average can better account for TME heterogeneity and may be more representative of an entire tumor section, the immune hot spot core could better reveal subtle immune signatures of distinct T cell subtypes and infiltration levels that would have otherwise been attenuated or lost by averaging. Comparing the two workflows, the results were similar, especially in the univariate analysis, where none of the single markers was significant, while Treg cells were significantly associated with DFS

in both workflows. In the multivariate analysis, the results were comparable for the multi-marker classes, with Treg cells remaining significant, while the single markers were inconsistent between workflows. In addition, when using hierarchical clustering for the immune hot-spot core we were unable to discover a distinct immune signature that was significantly associated with survival (data not shown). Since the TMA cores were randomly selected from the tumor center, it is unknown whether the immune hot -pot represents the entire tumor or is random event. Considering these limitations, averaging may be a superior sampling approach for assessing tumor immune infiltration than selecting the hot-spot for the purposes of this study.

KRAS status has been reported to be a biomarker for outcome in MSS stage III CRC[20]. *KRAS* mutational status was not significantly associated with outcome in our study, although there was a non-significant association for improved DFS in the *KRAS* mutant group. *KRAS* mutation has been associated with an immunosuppressive TME in MSS CRC[21]. However, no differences were observed in the levels of any the T cell subtypes examined between *KRAS* WT and mutant tumors in our study.

In summary, we show that multiplexed analysis of tissue and multi-marker cell classification can be used to accurately determine immune cells in tumor and stroma in colorectal tumor cores. We also provide proof-of-concept evidence for its utility to identify highly specific immune subsets that have clinical relevance.

Supplementary information is available at *Modern Pathology's* website

References:

1 Locker GY, Hamilton S, Harris J, Jessup JM, Kemeny N, Macdonald JS, et al. ASCO 2006 update of recommendations for the use of tumor markers in gastrointestinal

cancer. J. Clin. Oncol. 2006;24:5313–5327.

2 André T, Boni C, Mounedji-Boudiaf L, Navarro M, Tabernero J, Hickish T, et al. Oxaliplatin, Fluorouracil, and Leucovorin as Adjuvant Treatment for Colon Cancer. N Engl J Med. 2004;350:2343–2351.

3 Auclin E, Zaanan A, Vernerey D, Douard R, Gallois C, Laurent-Puig P, et al. Subgroups and prognostication in stage III colon cancer: future perspectives for adjuvant therapy. Ann Oncol Off J Eur Soc Med Oncol. 2017;28:958–968.

4 Amin MB, Greene FL, Edge SB, Compton CC, Gershenwald JE, Brookland RK, et al. The Eighth Edition AJCC Cancer Staging Manual: Continuing to build a bridge from a population-based to a more “personalized” approach to cancer staging. CA Cancer J Clin. 2017;67:93–99.

5 Allen WL, Dunne PD, McDade S, Scanlon E, Loughrey M, Coleman HG, et al. Transcriptional Subtyping and CD8 Immunohistochemistry Identifies Patients With Stage II and III Colorectal Cancer With Poor Prognosis Who Benefit From Adjuvant Chemotherapy. JCO Precis Oncol. 2018;2:1–15.

6 Fridman WH, Pagès F, Sautès-Fridman C, Galon J. The immune contexture in human tumours: Impact on clinical outcome. Nat. Rev. Cancer. 2012;12:298–306.

7 Galon J, Pagès F, Marincola FM, Thurin M, Trinchieri G, Fox BA, et al. The immune score as a new possible approach for the classification of cancer. J. Transl. Med. 2012;10. doi:10.1186/1479-5876-10-1.

8 Nosho K, Baba Y, Tanaka N, Shima K, Hayashi M, Meyerhardt JA, et al. Tumour-infiltrating T-cell subsets, molecular changes in colorectal cancer, and prognosis: Cohort study and literature review. J Pathol. 2010;222:350–366.

9 Malka D, Lièvre A, André T, Taïeb J, Ducreux M, Bibeau F. Immune scores in colorectal cancer: Where are we? Eur. J. Cancer. 2020;140:105–118.

506 10 Sharma P, Allison JP. The future of immune checkpoint therapy. Science (80-).
507 2015;348:56–61.

508 11 Overman MJ, Lonardi S, Wong KYM, Lenz HJ, Gelsomino F, Aglietta M, et al. Durable
509 clinical benefit with nivolumab plus ipilimumab in DNA mismatch repair-
510 deficient/microsatellite instability-high metastatic colorectal cancer. J Clin Oncol.
511 2018;36:773–779.

512 12 Le DT, Uram JN, Wang H, Bartlett BR, Kemberling H, Eyring AD, et al. PD-1 blockade
513 in tumors with mismatch-repair deficiency. N Engl J Med. 2015;372:2509–2520.

514 13 Gerdes MJ, Sevinsky CJ, Sood A, Adak S, Bello MO, Bordwell A, et al. Highly
515 multiplexed single-cell analysis of formalinfixed, paraffin-embedded cancer tissue. Proc
516 Natl Acad Sci U S A. 2013;110:11982–11987.

517 14 Berens ME, Sood A, Barnholtz-Sloan JS, Graf JF, Cho S, Kim S, et al. Multiscale,
518 multimodal analysis of tumor heterogeneity in IDH1 mutant vs wild-type diffuse gliomas.
519 PLoS One. 2019;14. doi:10.1371/journal.pone.0219724.

520 15 Santamaria-Pang A, Padmanabhan RK, Sood A, Gerdes MJ, Sevinsky C, Li Q, et al.
521 Robust single cell quantification of immune cell subtypes in histological samples. In:
522 2017 IEEE EMBS International Conference on Biomedical and Health Informatics, BHI
523 2017. : Institute of Electrical and Electronics Engineers Inc., 2017. p. 121–124.

524 16 Padfield D, Rittscher J, Roysam B. Coupled minimum-cost flow cell tracking. In: Lecture
525 Notes in Computer Science (including subseries Lecture Notes in Artificial Intelligence
526 and Lecture Notes in Bioinformatics). : Springer, Berlin, Heidelberg, 2009. p. 374–385.

527 17 Sood A, Sui Y, McDonough E, Santamaría-Pang A, Al-Kofahi Y, Pang Z, et al.
528 Comparison of multiplexed immunofluorescence imaging to chromogenic
529 immunohistochemistry of skin biomarkers in response to monkeypox virus infection.
530 Viruses. 2020;12. doi:10.3390/v12080787.

18 Santamaria-Pang A, Rittscher J, Gerdes M, Padfield D. Cell segmentation and classification by hierarchical supervised shape ranking. In: Proceedings - International Symposium on Biomedical Imaging. : IEEE Computer Society, 2015. p. 1296–1299.

19 Santamaria-Pang A, Sood A, Meyer D, Chowdhury A, Ginty F. Automated Phenotyping via Cell Auto Training (CAT) on the Cell DIVE Platform. : Institute of Electrical and Electronics Engineers (IEEE), 2020. p. 2750–2756.

20 Taieb J, Le Malicot K, Shi Q, Penault-Llorca F, Bouché O, Tabernero J, et al. Prognostic Value of BRAF and KRAS Mutations in MSI and MSS Stage III Colon Cancer. J Natl Cancer Inst. 2017;109. doi:10.1093/jnci/djw272.

21 Marco M, Chen C-T, Choi S-H, Pelossof R, Shia J, Garcia-Aguilar J. A KRAS mutation is associated with an immunosuppressive tumor microenvironment in mismatch-repair proficient colorectal cancer. J Clin Oncol. 2019;37:609–609.

22 Sztupinszki Z, Gyorffy B. Colon cancer subtypes: Concordance, effect on survival and selection of the most representative preclinical models. Sci Rep. 2016;6:1–13.

23 Guinney J, Dienstmann R, Wang X, De Reyniès A, Schlicker A, Soneson C, et al. The consensus molecular subtypes of colorectal cancer. Nat Med. 2015;21:1350–1356.

24 Isella C, Brundu F, Bellomo SE, Galimi F, Zanella E, Porporato R, et al. Selective analysis of cancer-cell intrinsic transcriptional traits defines novel clinically relevant subtypes of colorectal cancer. Nat Commun. 2017;8. doi:10.1038/ncomms15107.

25 Song N, Pogue-Geile KL, Gavin PG, Yothers G, Kim SR, Johnson NL, et al. Clinical outcome from oxaliplatin treatment in stage II/III colon cancer according to intrinsic subtypes: Secondary analysis of NSABP C-07/NRG oncology randomized clinical trial. In: JAMA Oncology. : American Medical Association, 2016. p. 1162–1169.

26 Shevyrev D, Tereshchenko V. Treg Heterogeneity, Function, and Homeostasis. Front. Immunol. 2020;10. doi:10.3389/fimmu.2019.03100.

556 27 Chen W, Konkel JE. Development of thymic Foxp3+ regulatory T cells: TGF-β matters.
557 Eur. J. Immunol. 2015;45:958–965.

558 28 Lui PPW, Cho I, Ali N. Tissue regulatory T cells. Immunology. 2020;161:4–17.

559 29 Mekori YA, Hershko AY. T cell-mediated modulation of mast cell function: Heterotypic
560 adhesion-induced stimulatory or inhibitory effects. Front. Immunol. 2012;3.
561 doi:10.3389/fimmu.2012.00006.

562 30 Gliwiński M, Iwaszkiewicz-Grześ D, Trzonkowski P. Cell-Based Therapies with T
563 Regulatory Cells. BioDrugs. 2017;31:335–347.

564 31 Khaja ASS, Toor SM, Salhat HE, Ali BR, Elkord E. Intratumoral FoxP3+Helios+
565 regulatory T Cells upregulating immunosuppressive molecules are expanded in human
566 colorectal cancer. Front Immunol. 2017;8. doi:10.3389/fimmu.2017.00619.

567 32 Curotto de Lafaille MA, Lafaille JJ. Natural and Adaptive Foxp3+ Regulatory T Cells:
568 More of the Same or a Division of Labor? Immunity. 2009;30:626–635.

569 33 Plitas G, Konopacki C, Wu K, Bos PD, Morrow M, Putintseva E V., et al. Regulatory T
570 Cells Exhibit Distinct Features in Human Breast Cancer. Immunity. 2016;45:1122–
571 1134.

572 34 Chen WJ, Jin W, Hardegen N, Lei KJ, Li L, Marinos N, et al. Conversion of Peripheral
573 CD4+CD25- Naive T Cells to CD4+CD25+ Regulatory T Cells by TGF-β Induction of
574 Transcription Factor Foxp3. J Exp Med. 2003;198:1875–1886.

575 35 Yaqub S, Henjum K, Mahic M, Jahnsen FL, Aandahl EM, Bjørnbeth BA, et al.
576 Regulatory T cells in colorectal cancer patients suppress anti-tumor immune activity in
577 a COX-2 dependent manner. Cancer Immunol Immunother. 2008;57:813–821.

578 36 Wang Z, Hua W, Li C, Chang H, Liu R, Ni Y, et al. Protective Role of Fecal Microbiota
579 Transplantation on Colitis and Colitis-Associated Colon Cancer in Mice Is Associated
580 With Treg Cells. Front Microbiol. 2019;10. doi:10.3389/fmicb.2019.02498.

581 37 Schmidt A, Oberle N, Krammer PH. Molecular mechanisms of Treg-mediated T cell
582 suppression. Front. Immunol. 2012;3. doi:10.3389/fimmu.2012.00051.

583 38 Mowat AM, Agace WW. Regional specialization within the intestinal immune system.
584 Nat. Rev. Immunol. 2014;14:667–685.

585 39 Zhuo C, Li Z, Xu Y, Wang Y, Li Q, Peng J, et al. Higher FOXP3-TSDR demethylation
586 rates in adjacent normal tissues in patients with colon cancer were associated with
587 worse survival. Mol Cancer. 2014;13:153.

588 40 Zhu X wen, Zhu H zhen, Zhu Y qing, Feng M hui, Qi J, Chen Z fen. Foxp3 expression
589 in CD4+CD25+Foxp3+ regulatory T cells promotes development of colorectal cancer
590 by inhibiting tumor immunity. J Huazhong Univ Sci Technol - Med Sci. 2016;36:677–
591 682.

592 41 Correale P, Rotundo MS, Del Vecchio MT, Remondo C, Migali C, Ginanneschi C, et al.
593 Regulatory (FoxP3+) T-cell tumor infiltration is a favorable prognostic factor in
594 advanced colon cancer patients undergoing chemo or chemoimmunotherapy. J
595 Immunother. 2010;33:435–441.

596 42 Hu G, Li Z, Wang S. Tumor-infiltrating FoxP3+ Tregs predict favorable outcome in
597 colorectal cancer patients: A meta-analysis. Oncotarget. 2017;8:75361–75371.

598 43 Frey DM, Droeser RA, Viehl CT, Zlobec I, Lugli A, Zingg U, et al. High frequency of
599 tumor-infiltrating FOXP3 $^{+}$ regulatory T cells predicts improved survival in mismatch
600 repair-proficient colorectal cancer patients. Int J Cancer. 2010;126:NA-NA.

601 44 Xu P, Fan W, Zhang Z, Wang J, Wang P, Li Y, et al. The clinicopathological and
602 prognostic implications of FoxP3+ regulatory T cells in patients with colorectal cancer:
603 A meta-analysis. Front Physiol. 2017;8. doi:10.3389/fphys.2017.00950.

604 45 Saito T, Nishikawa H, Wada H, Nagano Y, Sugiyama D, Atarashi K, et al. Two FOXP3
605 + CD4 + T cell subpopulations distinctly control the prognosis of colorectal cancers. Nat

606 Med. 2016;22:679–684.

607 46 Gooden MJM, De Bock GH, Leffers N, Daemen T, Nijman HW. The prognostic influence
608 of tumour-infiltrating lymphocytes in cancer: A systematic review with meta-analysis.
609 Br. J. Cancer. 2011;105:93–103.

610 47 Wang J, Ioan-Facsinay A, van der Voort EIH, Huizinga TWJ, Toes REM. Transient
611 expression of FOXP3 in human activated nonregulatory CD4+ T cells. Eur J Immunol.
612 2007;37:129–138.

613 48 Allan SE, Crome SQ, Crellin NK, Passerini L, Steiner TS, Bacchetta R, et al. Activation-
614 induced FOXP3 in human T effector cells does not suppress proliferation or cytokine
615 production. Int Immunol. 2007;19:345–354.

616 49 Elkord E, Al Samid MA, Chaudhary B. Helios, and not FoxP3, is the marker of activated
617 Tregs expressing GARP/LAP. Oncotarget. 2015;6:20026–20036.

618 50 Scurr M, Ladell K, Besneux M, Christian A, Hockey T, Smart K, et al. Highly prevalent
619 colorectal cancer-infiltrating LAP + Foxp3 - T cells exhibit more potent
620 immunosuppressive activity than Foxp3 + regulatory T cells. Mucosal Immunol.
621 2014;7:428–439.

622 51 Olguín JE, Medina-Andrade I, Rodríguez T, Rodríguez-Sosa M, Terrazas LI. Relevance
623 of regulatory T cells during colorectal cancer development. Cancers (Basel).
624 2020;12:1–19.

625 52 Dunne MR, Ryan C, Nolan B, Tosetto M, Geraghty R, Winter DC, et al. Enrichment of
626 inflammatory IL-17 and TNF-α secreting CD4+ T cells within colorectal tumors despite
627 the presence of elevated CD39+ T regulatory cells and increased expression of the
628 immune checkpoint molecule, PD-1. Front Oncol. 2016;6:50.

629 53 Toor SM, Murshed K, Al-Dhaheri M, Khawar M, Abu Nada M, Elkord E. Immune
630 Checkpoints in Circulating and Tumor-Infiltrating CD4+ T Cell Subsets in Colorectal

Cancer Patients. Front Immunol. 2019;10:2936.

54 Wherry EJ, Kurachi M. Molecular and cellular insights into T cell exhaustion. Nat. Rev. Immunol. 2015;15:486–499.

55 Lee WS, Park S, Lee WY, Yun SH, Chun HK. Clinical impact of tumor-infiltrating lymphocytes for survival in stage II colon cancer. Cancer. 2010;116:5188–5199.

Acknowledgements. Research reported in this publication was partially supported by the National Cancer Institute of the National Institutes of Health under award number R01CA208179 supporting FG, EMcD, AS, JG and AS-P and AC. DBL and XS were supported by a US-Ireland R01 award (NI Partner supported by HSCNI, STL/5715/15). JHMP is supported by Science Foundation Ireland and the Health Research Board (16/US/3301). ML is supported by Health Data Research UK

Conflict of Interest: ML has received honoraria from Pfizer, EMD Serono and Roche for presentations unrelated to this work. ML is supported by an unrestricted educational grant from Pfizer for research unrelated to this work.

LEGENDS OF FIGURES

Figure 1: A) Cell DIVE workflow: immunofluorescence staining with overlaying segmentation masks and resulting classification. Based on the classification data, an immune and stroma score was calculated per TMA core. **B**.) The immune score was calculated from the immune cell density as counts of segmented cells that were positive for any of the immune markers (CD45, CD3, CD4, CD8) in each core. The cores were grouped based on the pathologist's high-medium-low immune scores (x-axis) and each dot was the value of the Cell DIVE immune score (y-axis) per core. **C.)** The stroma score for each TMA core was calculated by counting segmented cells outside the epithelial mask that were negative for AE1 and immune markers,

and converting to 'percent of total' cells. The cores were grouped based on the pathologist's high-medium-low stroma scores (x-axis) and with each dot indicating stroma score (y-axis) per core. Statistical analysis was performed using Welch's ANOVA and pairwise t-test (***$P < 0.001$ for all comparisons).

Figure 2: A(a) Representative multiplexed immunofluorescent tissue images and segmentation masks that were used for the multi marker classification workflow. For single marker classification, the immune markers were assessed individually (CD3, CD4, CD8, FOXP3, PD1) and each cell was classified as positive or negative for each marker. **A(b)** Marker combination (AE1, CD3, CD4, CD8, FOXP3, PD1) was used for multi-marker classification workflow and based on the marker co-staining each cell was assigned a cell subtype as shown in the table. The eight multi marker T cell subtypes were: T helper cells (**Th**), T helper PD1 (**ThPD1**), T cytotoxic (**Tc**), T cytotoxic PD1+ (**TcPD1**), T regulatory (**Treg**), T regulatory PD1 positive (**TregPD1**), **Epithelial** and **Other** (non-lymphocyte, non-epithelial) cells**. A(c)** Illustration of the resulting multi-marker classification for the nuclear mask. **B)** Distribution of calculated values for % of Total for each T cell subtype, per patient. Each value represents the average of 2-3 assessable cores, per patient. **C)** Total counts from all patients grouped as epithelial-associated cells (red) and stromal cells (green) for each multi-marker T cell subtype. **D)** Correlation matrix showing the relationship between different T cell subtypes (Spearman's correlation coefficients). A color-coded correlation scale is provided and blue ellipses represent positive correlations, while darker color and narrower ellipses correspond to larger correlation coefficient magnitudes. E) Heatmap showing separation and clustering of patients based on % T cells of Total cells in tumor cores. Clusters based on the Ward.D agglomerative clustering method with Euclidean correlation distance measure.

Figure 3: Survival estimates for DFS and OS for **Average** of cores. Forest plots for multi-marker classification (Tc, TcPD1, Th, ThPD1, Treg, TregPD1) and single-marker classification (CD3, CD4, CD8, FOXP3, PD1) for the patient cohort. Estimated HRs, 95% CIs, and p values from likelihood ratio tests from univariate Cox proportional hazards models demonstrated the

associations between the percent of total classified cells with the risks of recurrence (DFS) (**A**) **and** death (OS) (**B**). In the multivariate analysis the biomarkers were adjusted for clinical variables (T, N, age, sex, nodal count, positive nodes, differentiation, lymphovascular invasion) for DFS (**C**) and OS (**D**). Kaplan–Meier curves demonstrating univariate survival analysis for percent of total for Treg dichotomized at the median for DFS (**E**) and OS (**F**). Differences in Kaplan–Meier survival curves are presented as log- rank P value.

Figure 4: Survival estimates for DFS and OS for **immune hot-spot**: Forest plots for multi-marker classification (Tc, TcPD1, Th, ThPD1, Treg, TregPD1) and single-marker classification (CD3, CD4, CD8, FOXP3, PD1) for the patient cohort. Estimated HRs, 95% CIs, and P values from likelihood ratio tests from univariate Cox proportional hazards models demonstrated the associations between the percent of total classified cells with the risks of recurrence (DFS) (**A**) and death (OS) (**B**). In the multivariate analysis the biomarkers were adjusted for clinical variables (T, N, age, sex, nodal count, positive nodes, differentiation, lymphovascular invasion) for DFS (**C**) and OS (**D**).

Supplementary Figure 1: Panel of representative multiplexed image with the corresponding segmentation masks and individual staining for each antibody used for T cell classification and segmentation in this study.

Supplementary Figure 2: Heatmap showing separation and clustering of patients based on % T cells of Total T cell subtypes in tumor cores. Clusters based on the Ward.D agglomerative clustering method with Euclidean correlation distance measure. Kaplan-Meier curves color-coded for the corresponding 2 (A) and 3 (B) clusters of patients, demonstrating univariate survival analysis for DFS and OS. Differences in Kaplan–Meier survival curves are presented as log- rank p value.

Supplementary Figure 3: Pearson Correlation between cell counts for single marker model and multi marker classification. **CD3**: CD3 vs Tc+TcPD1+Th+ThPD1+Treg+TregPD1, **CD4**: CD4 vs Th+ThPD1+Treg+TregPD1, **CD8**: CD8 vs Tc+TcPD1, **FOXP3**: FOXP3 vs

709 Treg+TregPD1, **PD1**: PD1 vs TcPD1+ThPD1+TregPD1. The average counts of % of Total per
710 patient were used for the analysis.

711 **Supplementary Figure 4:** Representative vHE images and the corresponding multiplexed
712 immunofluorescence and tissue mappings after classification.

713 **Supplementary Figure 5:** Forest plots of multivariate Cox proportional hazards models for
714 clinical variables after backward elimination.

715 **Supplementary Figure 6:** Univariate survival analysis using Kaplan-Meier curves for single-
716 marker and multi-marker T cell subtypes as percent of Total for average. The patients were
717 separated in two groups using the median as cut-off.

718 **Supplementary Figure 7:** Univariate survival analysis using Kaplan-Meier curves for single-
719 marker and multi-marker T cell subtypes as percent of Total for immune hot-spot cores. The
720 patients were separated in two groups using the median as cut-off.

721 **Supplementary Figure 8: A)** Association of Kras status with survival for treated patients for
722 DFS and OS.

723

724

A

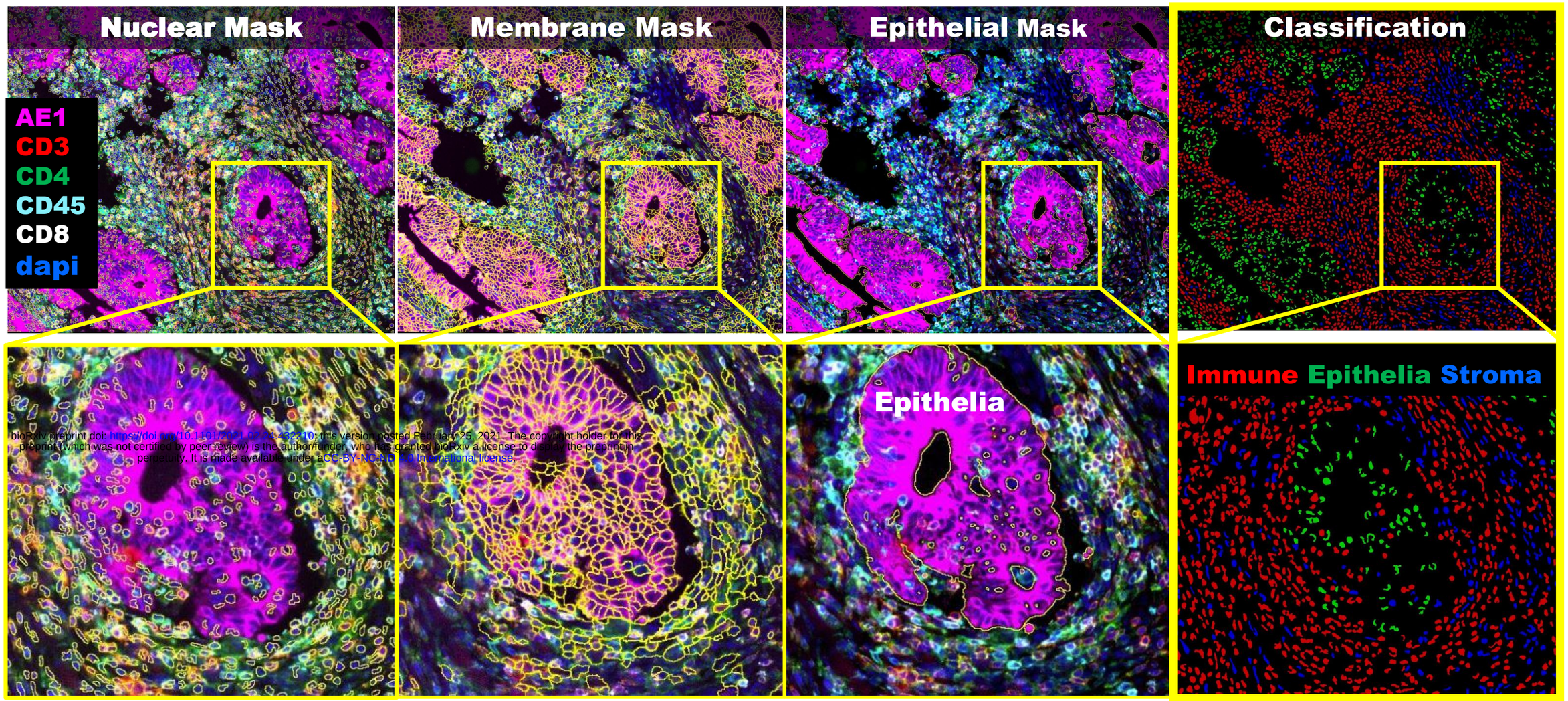

B

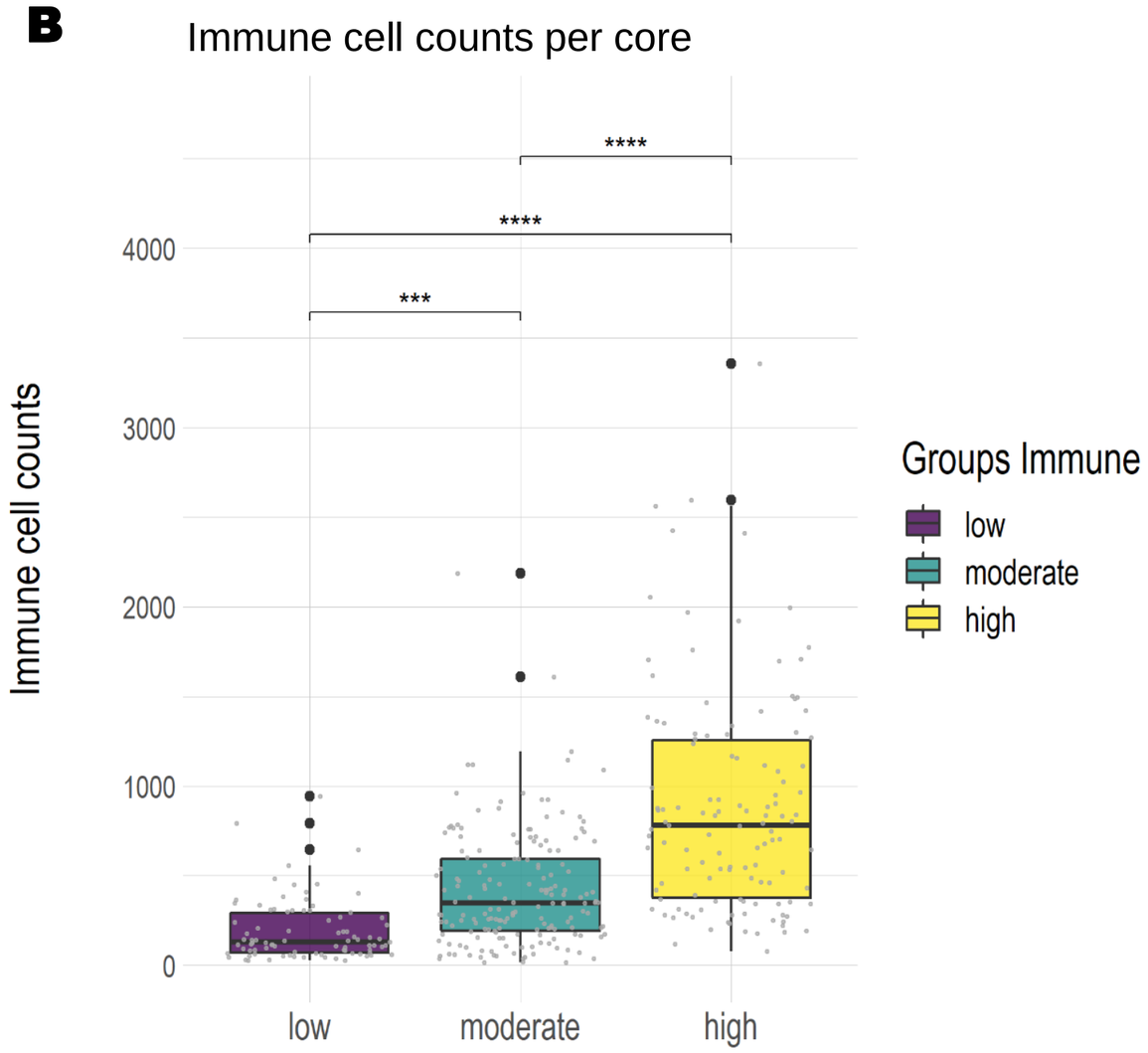

C

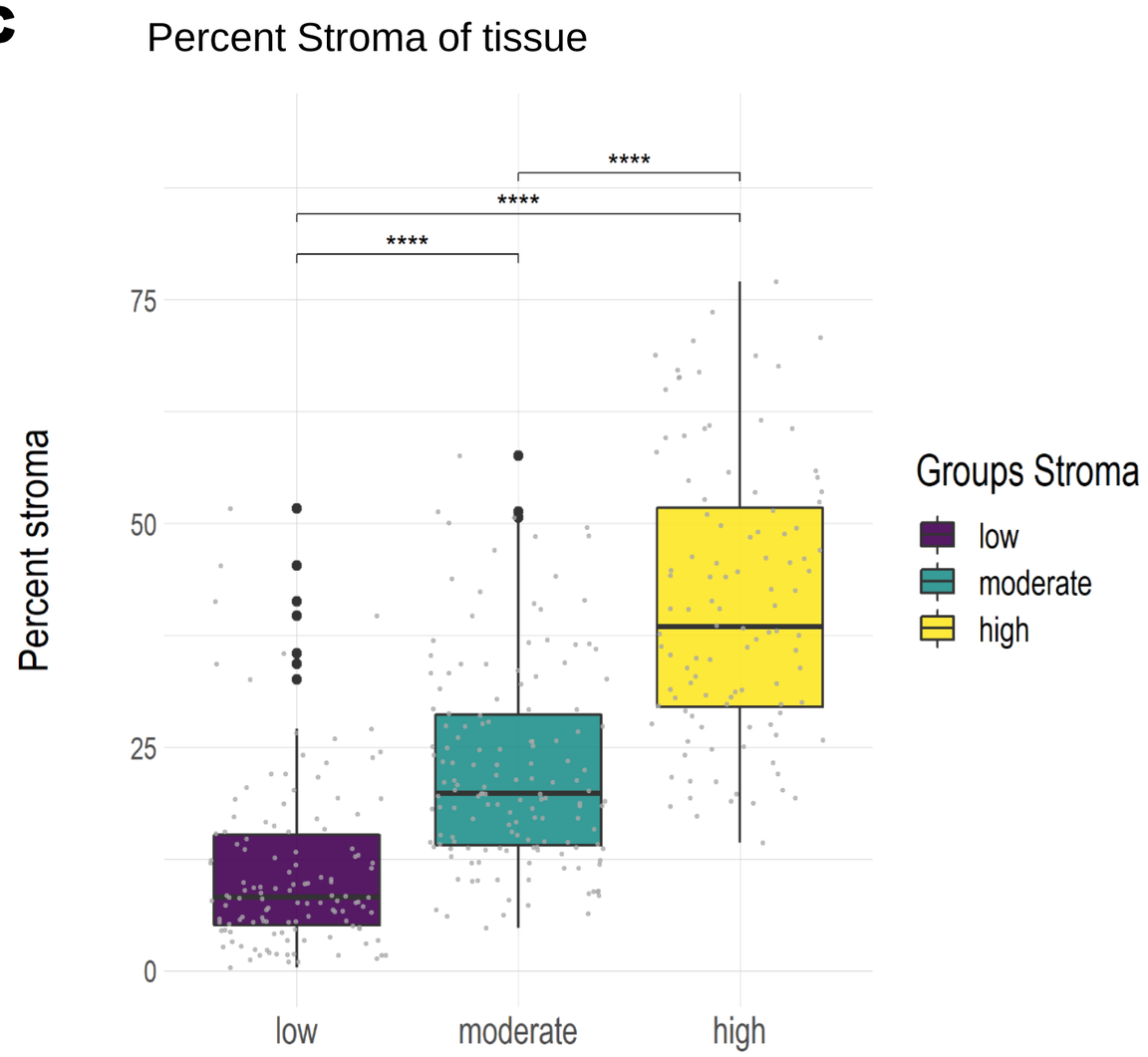

A

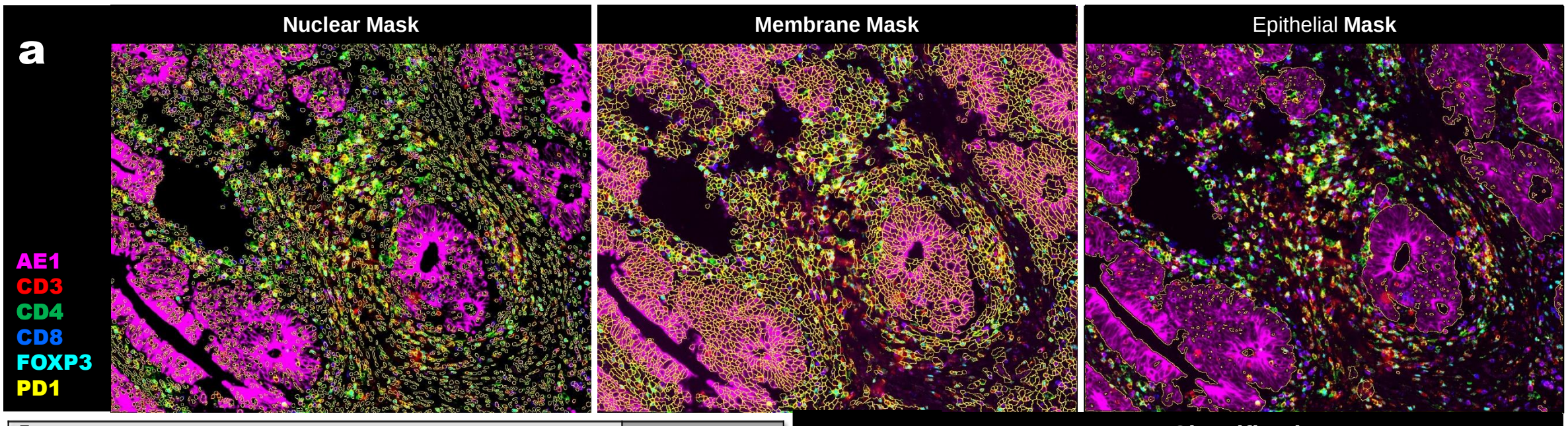

b

MARKERS						Cell Phenotype
AE1	CD3	CD4	CD8	FOXP3	PD1	
-	+	+	-	-	-	Th
-	+	+	-	-	+	ThPD1
-	+	-	+	-	-	Tc
-	+	-	+	-	+	TcPD1
-	+	+	-	+	-	Treg
-	+	+	-	+	+	TregPD1
-	+	-	-	-	-	Other
+	-	-	-	-	-	Epithelia

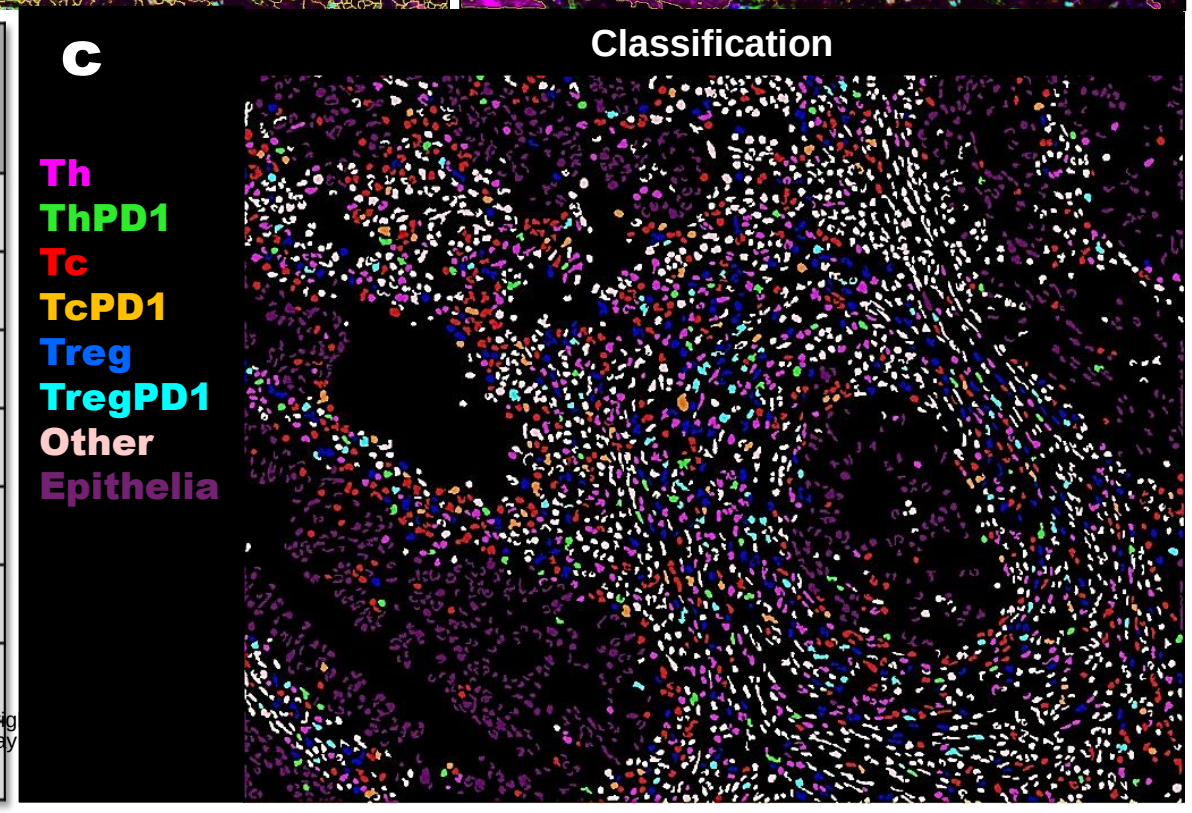

B

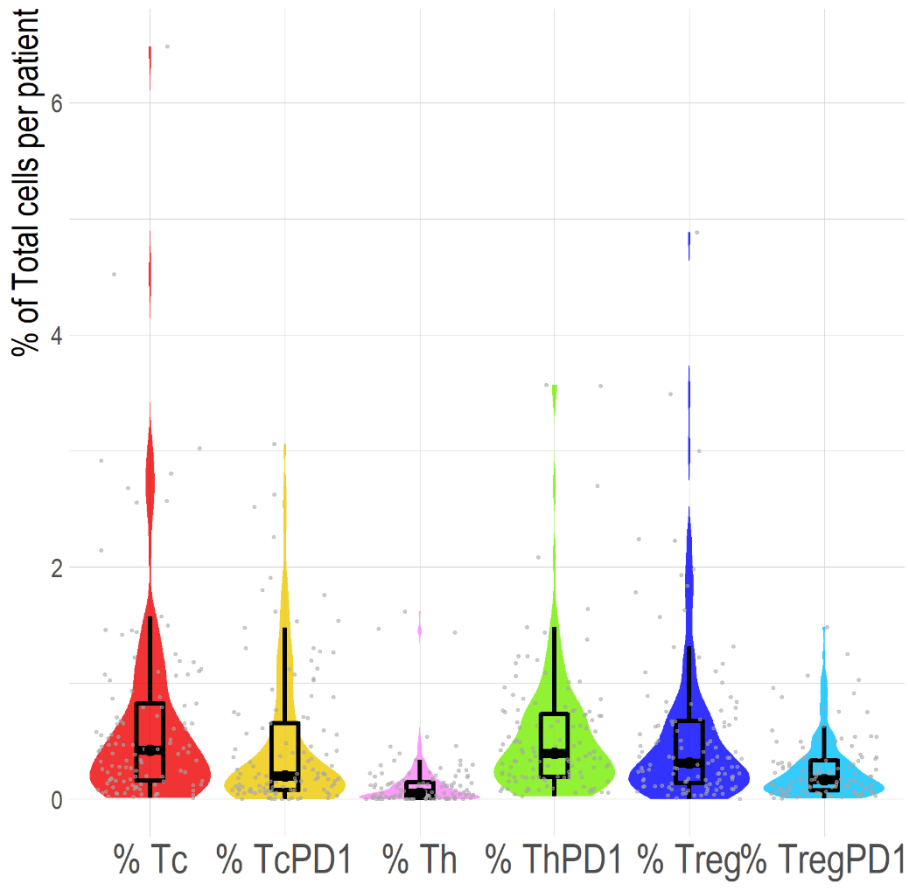

C

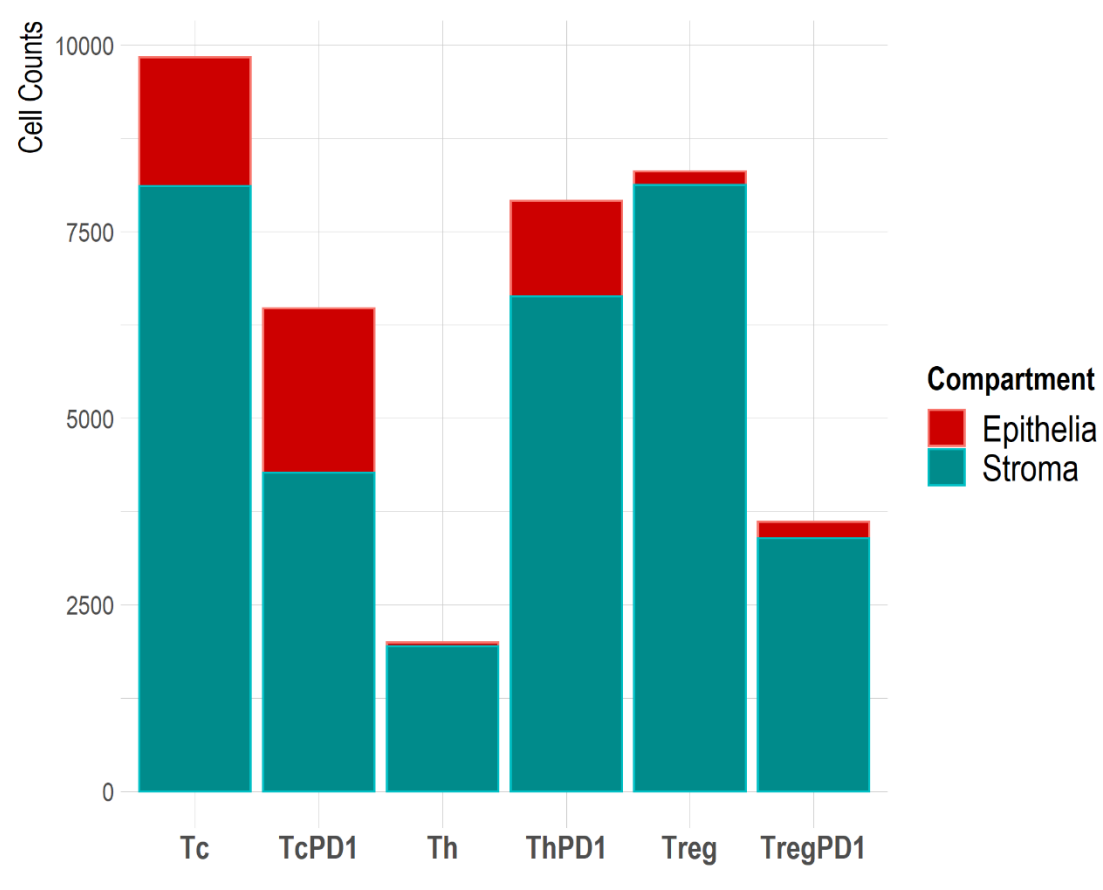

D

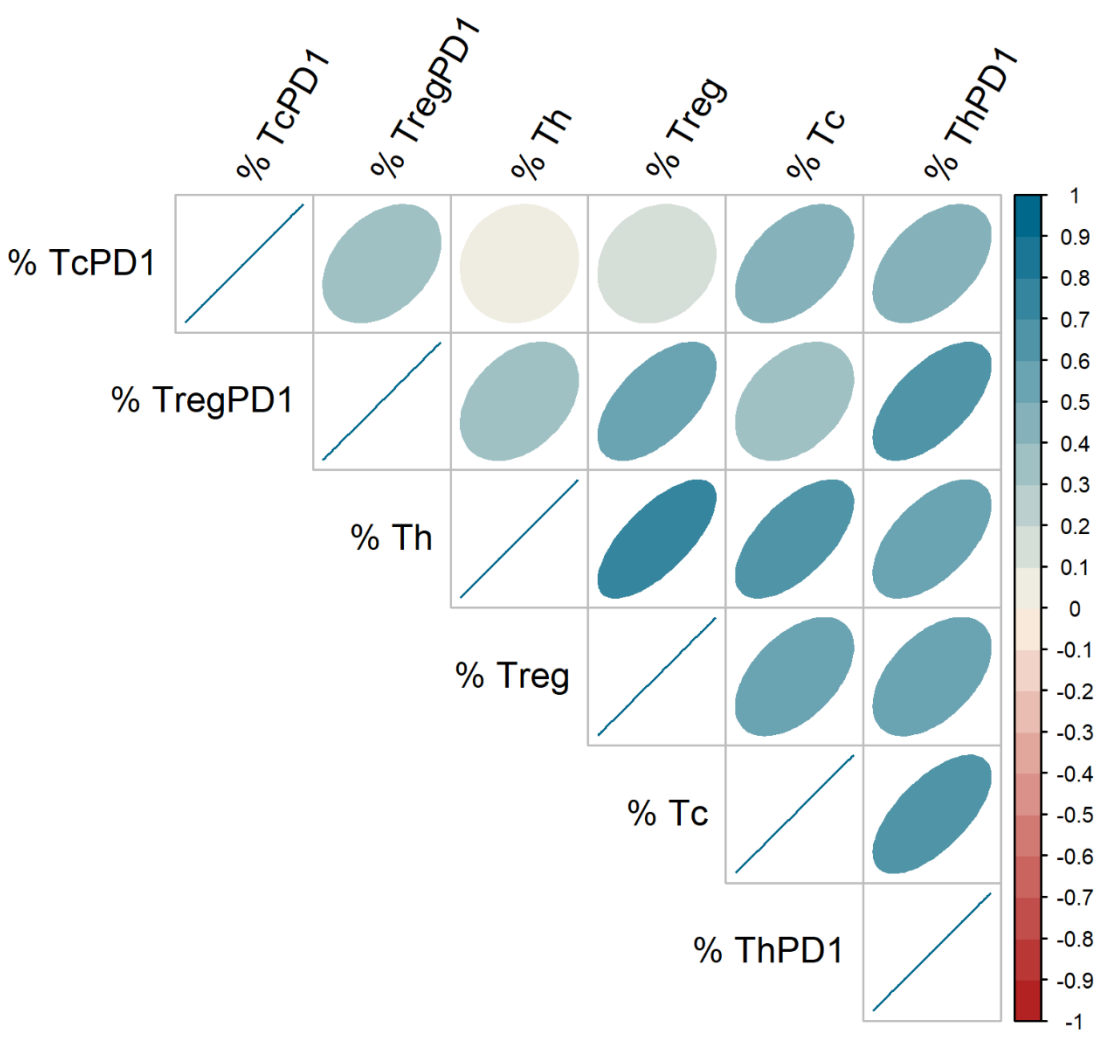

E

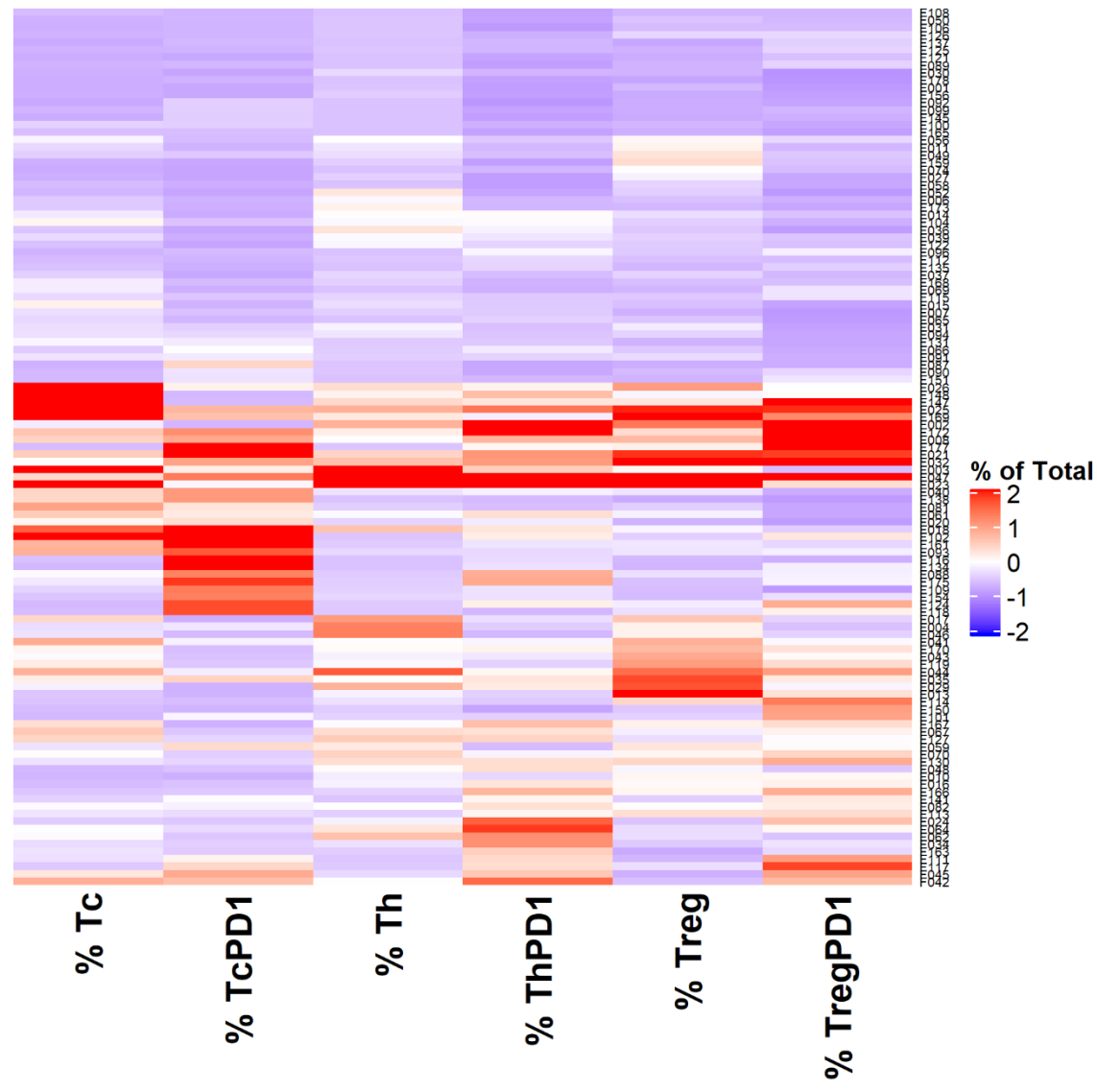

A

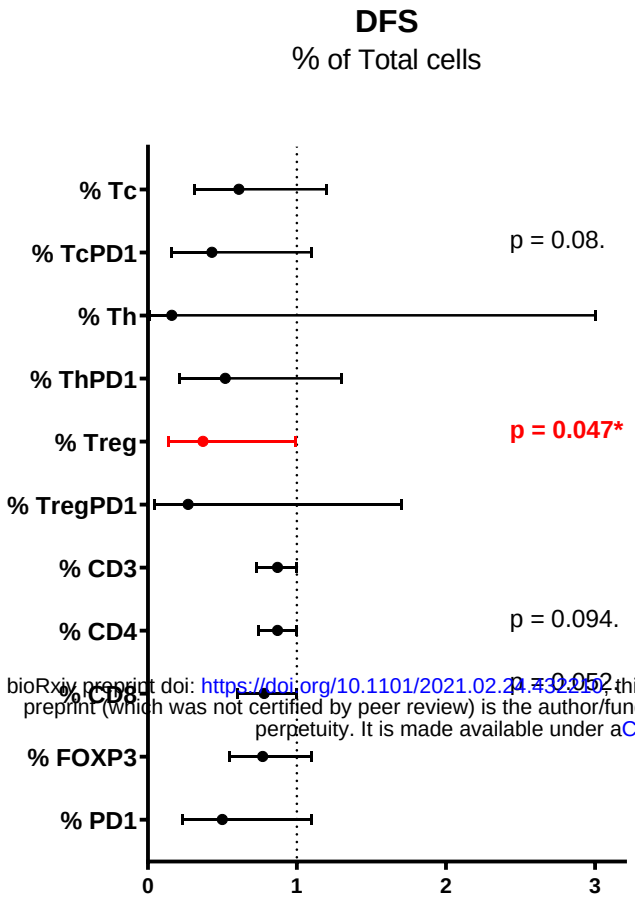

B

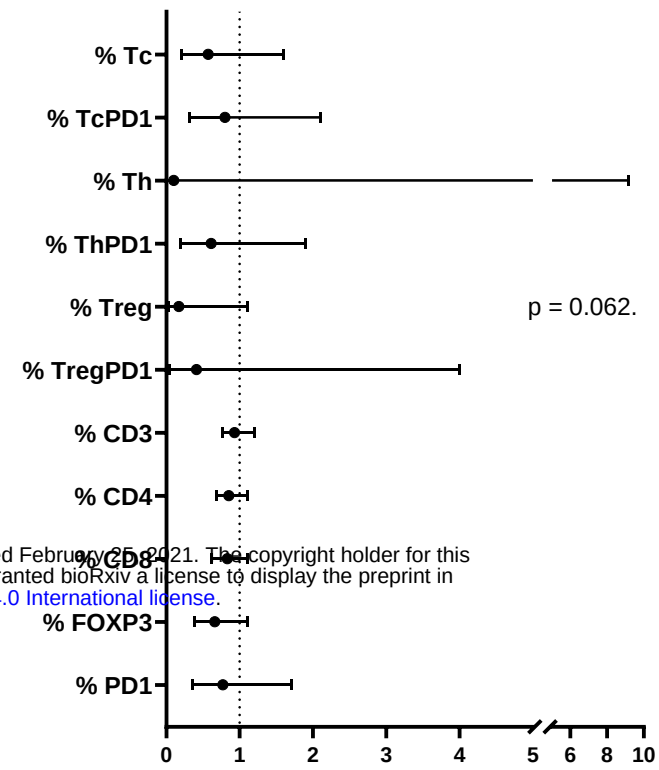

C

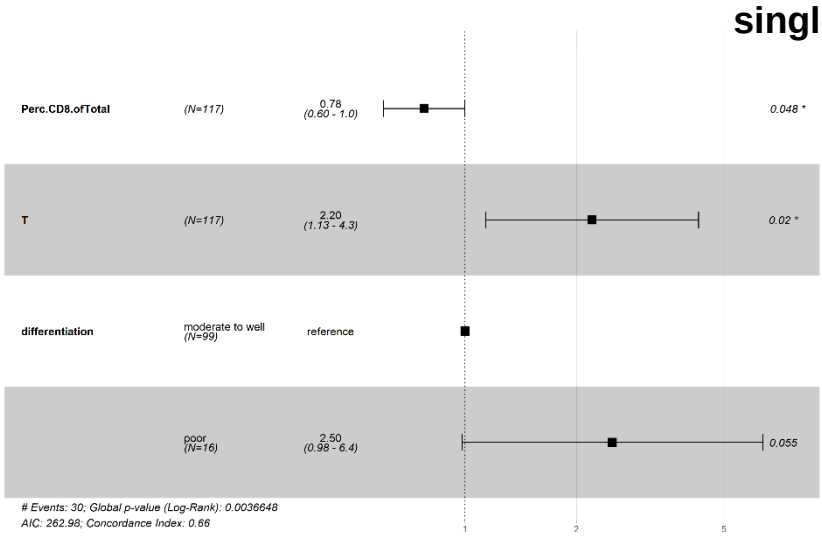

D

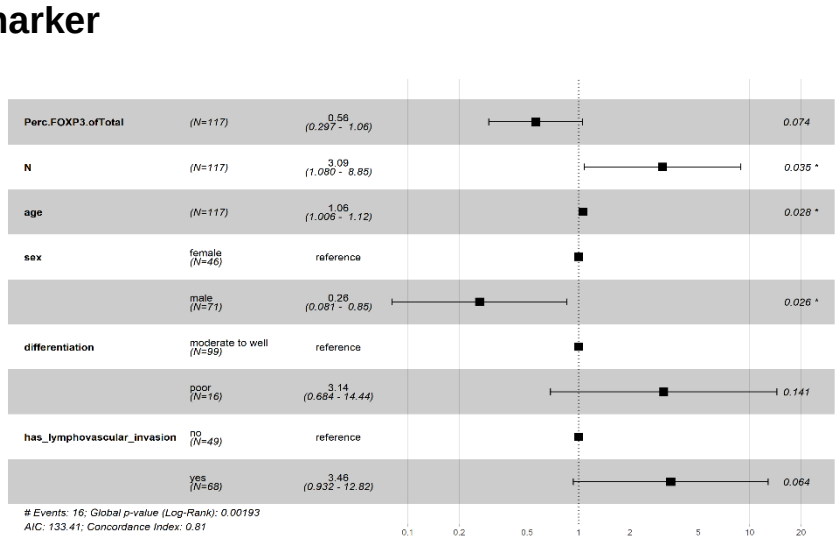

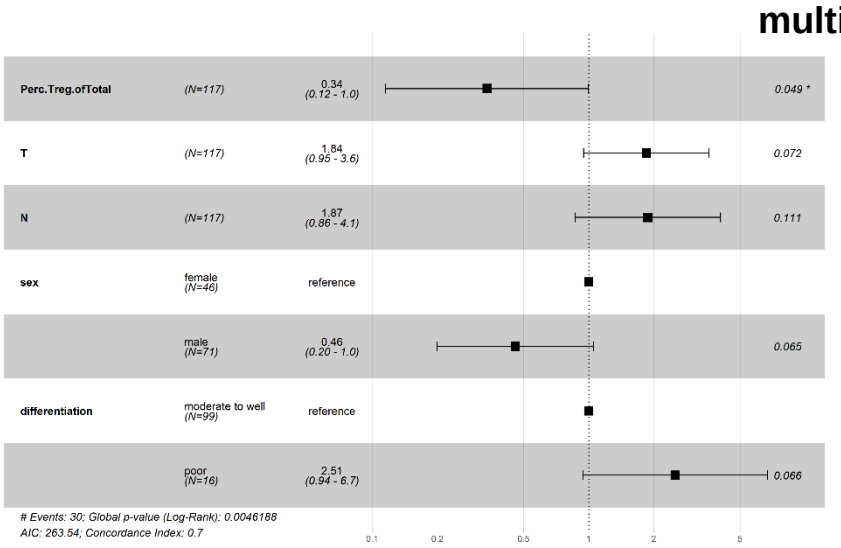

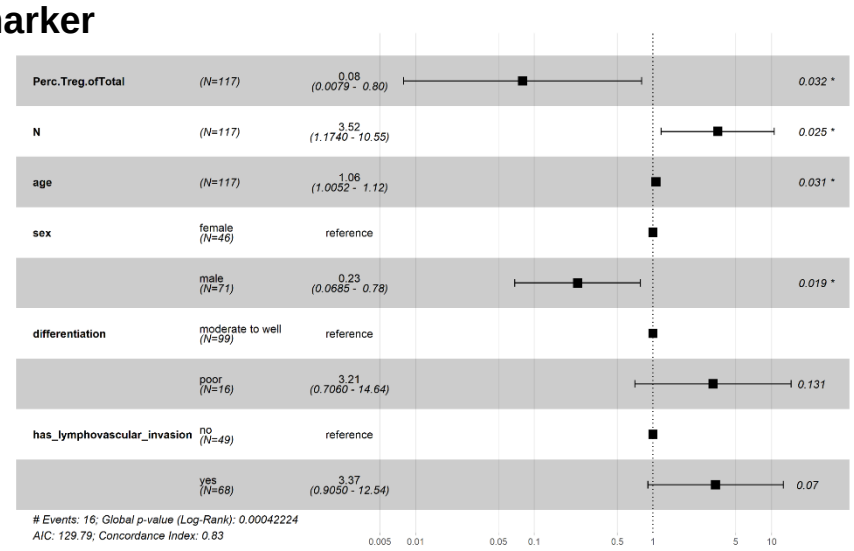

E

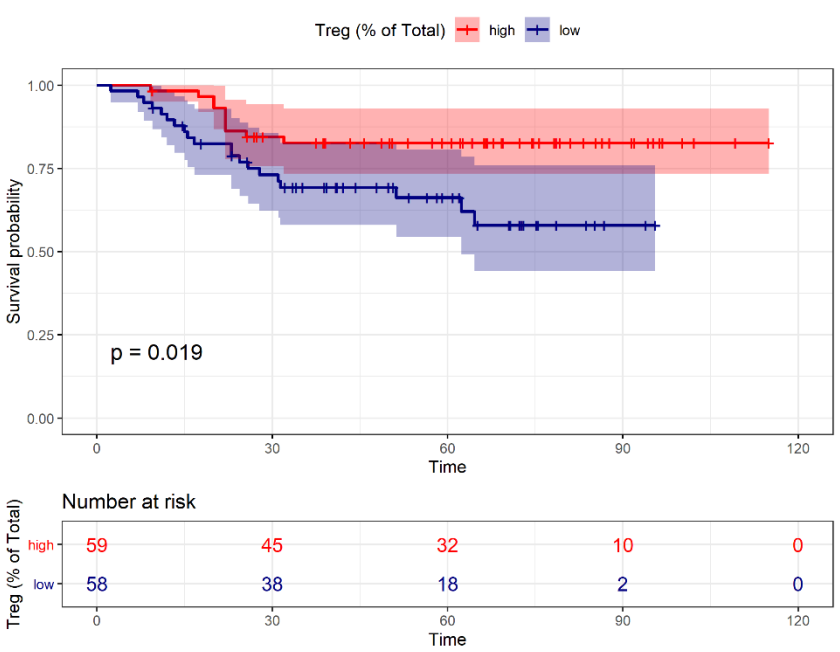

F

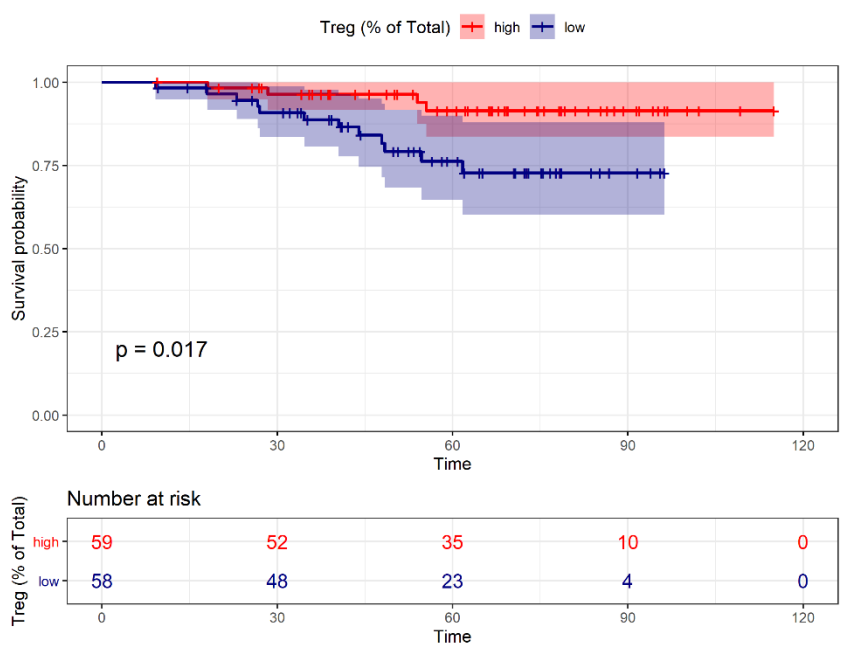

A

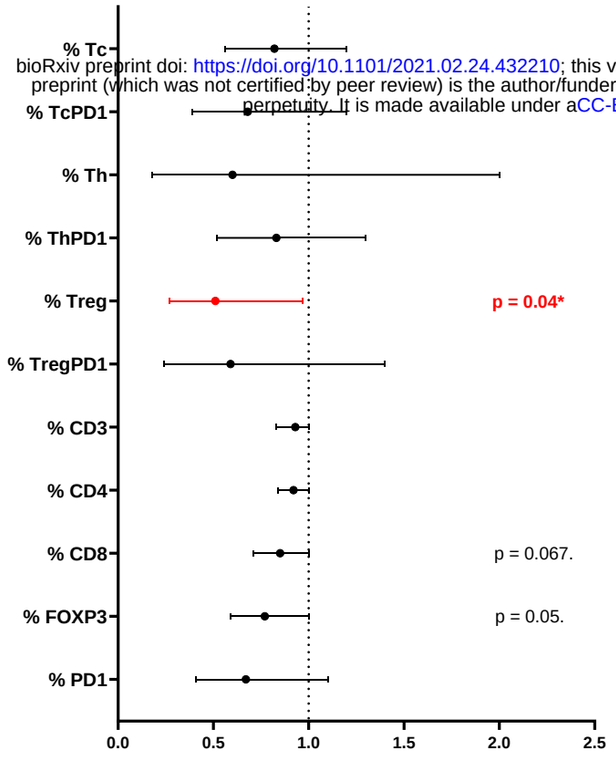

B

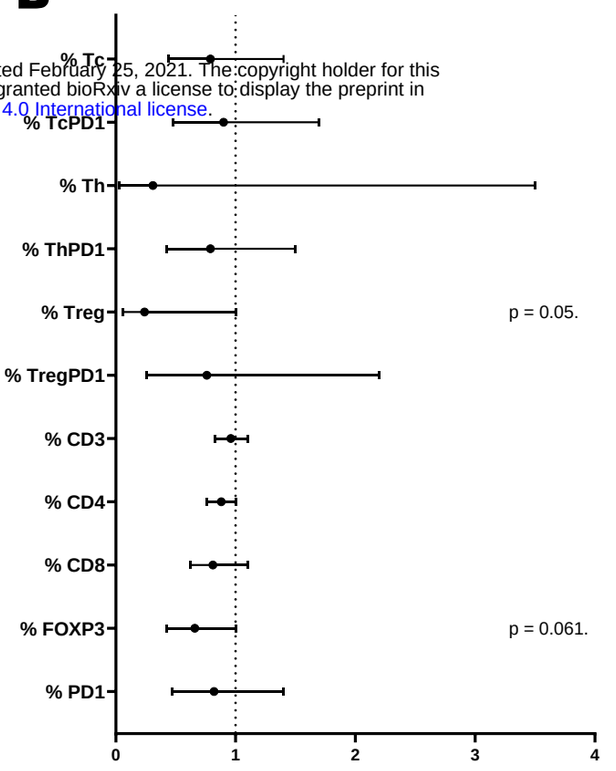

C

DFS

single-marker

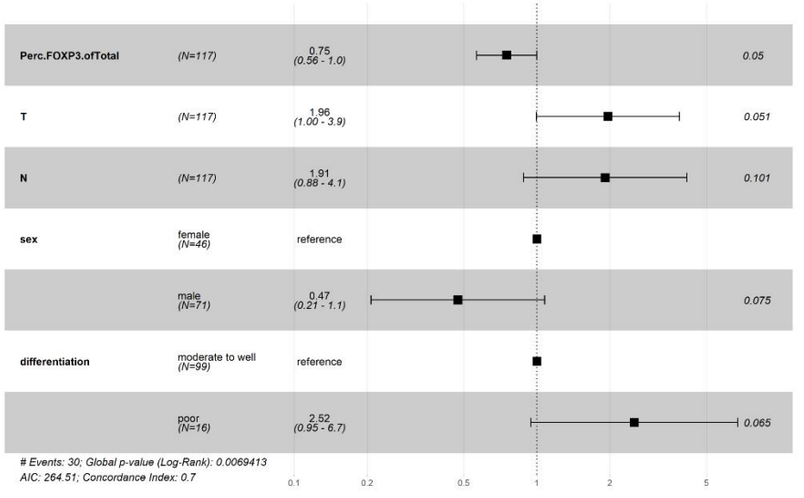

multi-marker

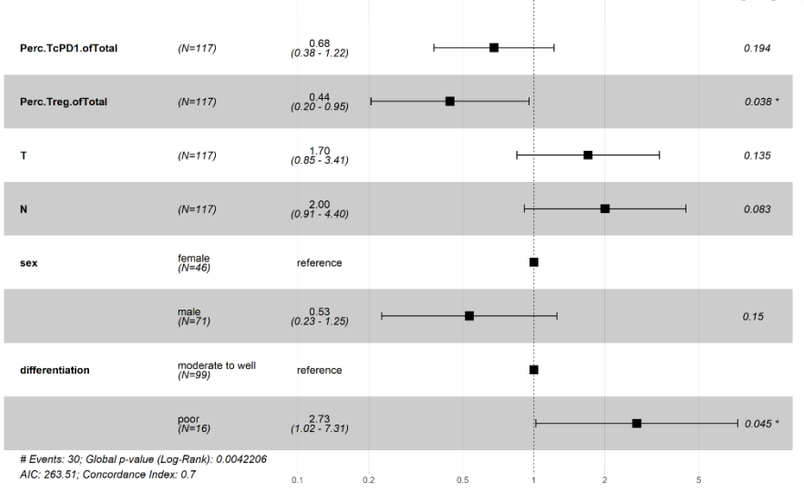

D

OS

single-marker

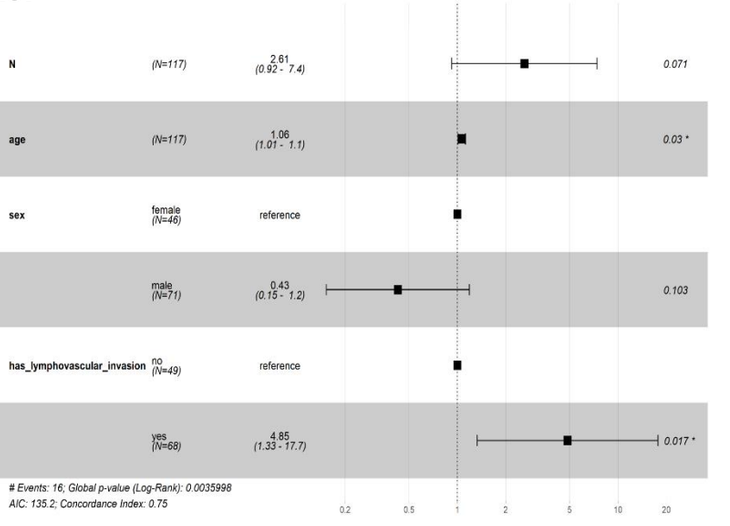

multi-marker

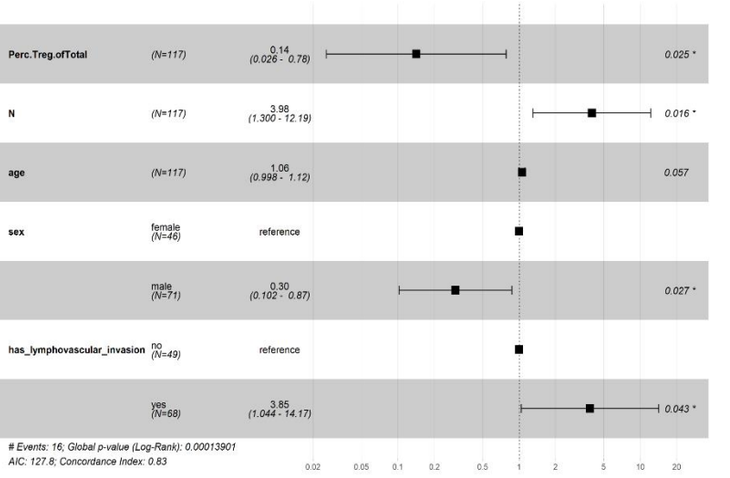

Table 1: Demographic data of patient cohort

	Overall (N=117)
DFS (months)	
Mean (SD)	51.7 (27.9)
Median [Min, Max]	50.7 [2.40, 115]
OS (months)	
Mean (SD)	58.5 (24.7)
Median [Min, Max]	59.1 [9.20, 115]
sex	
female	46 (39.3%)
male	71 (60.7%)
T	
2	10 (8.5%)
3	70 (59.8%)
4	37 (31.6%)
N	
1	83 (70.9%)
2	34 (29.1%)
age (years)	
Mean (SD)	59.2 (11.2)
Median [Min, Max]	61.0 [26.0, 79.0]
LNC	
Mean (SD)	21.3 (11.0)
Median [Min, Max]	19.0 [5.00, 73.0]
PLN	
Mean (SD)	3.05 (2.49)
Median [Min, Max]	2.00 [1.00, 13.0]
LVI	
no	49 (41.9%)
yes	68 (58.1%)
differentiation	
moderate to well	99 (84.6%)
poor	16 (13.7%)

*LNC=Lymph Node Count, *PLN=Positive Lymph Nodes, *LVI=Lymphovascular Invasion

Table 2: Summary statistics for multi-marker and single-marker subtypes.

	Overall (N=117)
% Tc (of total cells)	
Mean (SD)	0.693 (0.925)
Median [Min, Max]	0.423 [0.0111, 6.49]
% TcPD1	
Mean (SD)	0.477 (0.619)
Median [Min, Max]	0.197 [0, 3.06]
% Th	
Mean (SD)	0.133 (0.251)
Median [Min, Max]	0.0511 [0, 1.62]
% ThPD1	
Mean (SD)	0.559 (0.593)
Median [Min, Max]	0.394 [0.0222, 3.57]
% Treg	
Mean (SD)	0.568 (0.732)
Median [Min, Max]	0.312 [0, 4.88]
% TregPD1	
Mean (SD)	0.262 (0.275)
Median [Min, Max]	0.166 [0.00471, 1.48]
% CD3	
Mean (SD)	3.18 (2.88)
Median [Min, Max]	2.52 [0.221, 22.3]
% CD4	
Mean (SD)	3.64 (3.52)
Median [Min, Max]	2.67 [0.126, 23.3]
% CD8	
Mean (SD)	2.17 (2.42)
Median [Min, Max]	1.35 [0.0283, 12.3]
% FOXP3	
Mean (SD)	1.58 (1.46)
Median [Min, Max]	1.19 [0.0114, 8.57]
% PD1	
Mean (SD)	0.669 (0.694)
Median [Min, Max]	0.395 [0.00943, 3.41]

Table 3: Demographic data and summary statistics of multi-marker model based on KRAS status

	WT (N=64)	mutant (N=44)	p-value
sex			
female	24 (37.5%)	20 (45.5%)	0.53
male	40 (62.5%)	24 (54.5%)	
T			
2	4 (6.2%)	6 (13.6%)	0.342
3	37 (57.8%)	26 (59.1%)	
4	23 (35.9%)	12 (27.3%)	
N			
1	42 (65.6%)	34 (77.3%)	0.277
2	22 (34.4%)	10 (22.7%)	
age scores			
<50	18 (28.1%)	7 (15.9%)	0.296
>70	14 (21.9%)	7 (15.9%)	
51-60	11 (17.2%)	11 (25.0%)	
61-70	21 (32.8%)	19 (43.2%)	
LNC			
<12	8 (12.5%)	5 (11.4%)	0.919
>20	28 (43.8%)	21 (47.7%)	
Dec-20	28 (43.8%)	18 (40.9%)	
PLN			
N>7	6 (9.4%)	2 (4.5%)	0.393
N1-3	42 (65.6%)	34 (77.3%)	
N4-6	16 (25.0%)	8 (18.2%)	
LVI			
no	21 (32.8%)	23 (52.3%)	0.0683
yes	43 (67.2%)	21 (47.7%)	
% Tc (of total cells)			
Mean (SD)	0.636 (0.728)	0.848 (1.20)	0.355
Median [Min, Max]	0.421 [0.0111, 3.02]	0.475 [0.0199, 6.49]	
% TcPD1			
Mean (SD)	0.550 (0.670)	0.411 (0.546)	0.606
Median [Min, Max]	0.215 [0, 3.06]	0.254 [0, 2.63]	
% Th			
Mean (SD)	0.107 (0.215)	0.191 (0.309)	0.0721
Median [Min, Max]	0.0393 [0, 1.62]	0.115 [0, 1.47]	
% ThPD1			
Mean (SD)	0.547 (0.538)	0.634 (0.695)	0.63
Median [Min, Max]	0.407 [0.0222, 3.56]	0.416 [0.0564, 3.57]	
% Treg			
Mean (SD)	0.525 (0.669)	0.680 (0.862)	0.371
Median [Min, Max]	0.303 [0.0319, 3.49]	0.352 [0.00996, 4.88]	
% TregPD1			
Mean (SD)	0.287 (0.312)	0.245 (0.227)	0.778
Median [Min, Max]	0.182 [0.00471, 1.48]	0.166 [0.0253, 0.910]	

*LNC=Lymph Node Count, *PLN=Positive Lymph Nodes, *LVI=Lymphovascular Invasion